Maintenance of mitochondrial integrity in midbrain dopaminergic neurons governed by a conserved developmental transcription factor

Federico Miozzo[1,2], Luca Stickley[1], Eva P. Valencia-Alarcón[1], Michaela Dorcikova[1], Francesco Petrelli[3], Damla Tas[1,4], Nicolas Loncle[1,5], Irina Nikonenko[6], Peter Bou Dib[7,8] and Emi Nagoshi[1,*]

[1]Department of Genetics and Evolution and Institute of Genetics and Genomics of Geneva (iGE3), University of Geneva, CH-1211, Geneva 4, Switzerland

[2]Present address: Neuroscience Institute - CNR (IN-CNR), Milano, Italy

[3]Department of Cell Biology, University of Geneva, Geneva, Switzerland

[4]Present address: The Janssen Pharmaceutical Companies of Johnson & Johnson, Bern, Switzerland

[5]Present address: Puma Biotechnology, Inc., Berkeley, California

[6]Department of Basic Neurosciences and the Center for Neuroscience, CMU, University of Geneva, CH-1211, Geneva 4, Switzerland

[7]Institute of Cell Biology, University of Bern, CH-3012, Bern, Switzerland

[8]Present address: Department of Chemistry, Humboldt-Universität zu Berlin, 12489 Berlin, Germany

[*]Corresponding author: Emi.Nagoshi@unige.ch

ABSTRACT

The degeneration of dopaminergic (DA) neurons in the substantia nigra is a hallmark of Parkinson's disease (PD). Dysregulation of developmental transcription factors is implicated in dopaminergic neurodegeneration, but the underlying molecular mechanisms remain largely unknown. *Drosophila Fer2* is a prime example of a developmental transcription factor required for the birth and maintenance of midbrain DA neurons. Using an approach combining ChIP-seq, RNA-seq, and genetic epistasis experiments with PD-linked genes, here we demonstrate that *Fer2* controls a transcriptional network to maintain mitochondrial structure and function, and thus confers dopaminergic neuroprotection against genetic and oxidative insults. We further show that conditional ablation of *Nato3,* a mouse homolog of *Fer2*, in differentiated DA neurons results in locomotor impairments and mitochondrial abnormality in aged mice. Our results reveal the essential and conserved role of *Fer*2 homologs in the mitochondrial maintenance of midbrain DA neurons, opening new perspectives for modelling and treating PD.

INTRODUCTION

Midbrain dopaminergic (mDA) neurons play a central role in controlling key brain functions, including voluntary movement, associative learning, motivation and cognition[1]. The progressive and selective degeneration of mDA neurons in the substantia nigra (SN) results in a loss of nigrostriatal DA neurotransmission, leading to the motor symptoms of Parkinson's disease (PD). Although PD was first described over 200 years ago and is the most prevalent neurodegenerative movement disorder, the exact pathologic mechanisms underlying this disease remain unclear. Treatment options are limited to symptomatic relief with DA replacement therapy[2,3]. Thus, the identification of targets for disease-modifying therapies that reverse or hinder neurodegeneration in PD is greatly needed.

PD is a multifactorial disorder caused by a combination of genetic and environmental factors[4]. Increasing evidence indicates that PD risk factors lead to common pathological processes, including excessive production of reactive oxygen species (ROS), axonal pathology, neuroinflammation, defects in the ubiquitin-proteasome system, and mitochondrial dysfunction[5,2]. In particular, mitochondrial impairment is integral to most other pathological cellular processes and thought to play a central role in dopaminergic neurodegeneration. Complex I activity is reduced in the brains of PD patients, and mitochondrial toxins such as 1-methyl-4-phenyl-1,2,3,6-tetrahydropyridine (MPTP) and rotenone potently induce SN degeneration. The findings that multiple genes linked to familial PD, such as *PINK1*, *Parkin*, *LRRK2*, *SNCA* and *DJ-1*, directly or indirectly affect mitochondrial physiology further support this notion[6,7].

Although several genes linked to rare monogenic forms of PD have been identified, genetic susceptibility factors for sporadic PD, which accounts for approximately 90% of cases, remain largely unknown. In this regard, it is noteworthy that dysregulation of transcription factors required for mDA development is implicated in PD. Numerous

62 transcription factors required for various aspects of mDA neurons development, including
63 *En1*, *En2*, *Lmx1a*, *Lmx1b*, *Foxa1*, *Foxa2*, *Nurr1*, *Pitx3* and *Otx2*, remain expressed in the
64 adult brain and are crucial for the survival and function of differentiated mDA neurons in
65 mice[8–16]. Genome-wide association studies (GWAS) have shown that genetic variants of
66 developmental transcription factors are highly represented in sporadic PD patients[17,18].
67 Moreover, overexpression of *Nurr1*, *Foxa2*, *En1* or *Otx2* prevents the loss of DA neurons in
68 murine PD models[19–21]. Therefore, a better comprehension of the genetic networks controlled
69 by developmental transcription factors in differentiated mDA neurons may advance our
70 molecular understanding of neurodegeneration in PD and open new therapeutic options.
71 *Drosophila* offers a powerful model system to investigate molecular mechanisms of
72 PD pathogenesis *in vivo*, due to the abundance of genetic tools, the conservation of most PD-
73 related pathways and familial PD-linked genes, and its relatively simple nervous system[22,23].
74 The adult fly midbrain contains approximately a dozen clusters of DA neurons projecting to
75 different areas[24]. Although the anatomical arrangements of DA neurons in *Drosophila* and
76 vertebrates differ considerably, recent works have highlighted the functional homology of
77 some of the dopaminergic circuits[25]. The protocerebral anterior medial (PAM) cluster is the
78 largest subgroup containing approximately 80% of all *Drosophila* brain DA neurons. PAM
79 neurons are highly heterogeneous in their function and projection patterns, modulating
80 various behavior including associative learning, sleep, and locomotion[26,27]. Remarkably,
81 some of the PAM neurons are required for the startle-induced climbing, a locomotor behavior
82 found to be defective in multiple PD models[27–29], rendering the PAM cluster partially
83 analogous to the mammalian SN. Dopaminergic innervation from the PPL1 and PPM3
84 clusters to the central complex also appear to be functionally homologous to the nigrostriatal
85 pathway and is reported to be impaired in some PD models[25,30,31].
86 The notion that developmental transcription factors play critical roles in the

87 maintenance of adult DA neurons is shared between flies and mammals, as supported by our
88 recent studies of *Drosophila Fer2* gene[28]. *Fer2* encodes a basic helix-loop-helix (bHLH)
89 transcription factor required for the development of DA neurons in the PAM cluster, and
90 fewer PAM neurons are formed in $Fer2^2$ hypomorphic mutants. Additionally, $Fer2^2$ mutant
91 flies display a progressive loss of PAM neurons in adulthood, locomotor impairment that can
92 be improved by L-DOPA administration, and increased ROS levels in the brain. PAM
93 neurons deficient for *Fer2* accumulate abnormal mitochondria and show autophagy
94 dysfunction. *Fer2* expression persists into adulthood in PAM neurons and increases in
95 response to oxidative stress. Importantly, the maintenance of mitochondrial integrity and the
96 survival of PAM neurons in aged flies require the presence of *Fer2* in PAM neurons in
97 adulthood[28,29]. Taken together, these lines of evidence establish the dual role of *Fer2* in
98 development and lifelong maintenance of DA neurons in the PAM cluster, and suggest that
99 molecular studies of *Fer2* function will shed light on the mechanisms of dopaminergic
100 neurodegeneration relevant to PD.

101 In the present study, we ask how *Fer2* maintains DA neurons throughout adulthood
102 and whether its function is conserved in mammals. We address these questions by analyzing
103 functional interaction between *Fer2* and familial PD-linked genes, by identifying *Fer2* target
104 genes and by generating mice with a conditional deletion of *Nato3,* a murine homolog of
105 *Fer2*, in differentiated DA neurons. This combined approach demonstrates that *Fer2* is a
106 master regulator of a transcriptional network controlling mitochondrial integrity and function,
107 and thereby confers dopaminergic neuroprotection in multiple genetic and toxin models of
108 PD. *Nato3* is known to be required for the genesis of mDA neurons[32–34] but its post-
109 developmental role has never been studied. We show here for the first time that selective
110 ablation of *Nato3* in differentiated DA neurons leads to age-dependent motor impairment and
111 a loss of mitochondrial integrity in mDA neurons. Taken together, our results indicate that

112 *Fer2* and *Nato3* share an essential role in maintaining mitochondrial health and dopaminergic
113 function, offering new opportunities to study the selective vulnerability of mDA neurons and
114 to develop therapeutic interventions for PD.
115
116 **RESULTS**
117 ***Fer2* overexpression protects PAM dopaminergic neurons from genetic and oxidative**
118 **insults**
119 To explore the genetic mechanisms underlying the role of *Fer2* in the maintenance of DA
120 neurons, we investigated whether *Fer2* loss or gain of function affects the survival of DA
121 neurons in genetic models of PD. Mutations in the *leucine-rich repeat kinase 2* (*LRRK2*) gene
122 are the most common cause of familial PD and also predispose carriers to sporadic PD[35].
123 Because pathogenic *LRRK2* variants are considered to be gain-of-function mutants, most fly
124 models of *LRRK2*-linked PD employ overexpression of wild-type or mutant forms of *LRRK2*
125 or its fly homolog. We thus overexpressed wild-type or mutant *Drosophila Lrrk* via the
126 GAL4/UAS system using PAM neuron-specific drivers, *Fer2-GAL4* or *R58E02-GAL4*[26,28].
127 The number of surviving DA neurons was assessed by immunostaining with anti-tyrosine
128 hydroxylase (TH) antibodies.
129 Forced expression of either wild-type or *Lrrk I1915T* mutant, which is homologous to
130 the human pathogenic *LRRK2 I2020T* variant[35,36], reduced the number of TH-positive
131 neurons in the PAM cluster by approximately 10% in 1-day-old flies (Supplementary Fig.
132 1a). Thereafter TH-positive cell counts further decreased in an age-dependent manner
133 (Supplementary Fig. 1a and Fig. 1a, b). To distinguish the reduction in TH expression and the
134 genuine loss of DA neurons, we also visualized PAM neurons by expressing the nuclear
135 RedStinger red fluorescent protein together with *Lrrk*. The number of RedStinger-positive
136 cells was reduced in the flies expressing wild-type or mutant *Lrrk* in PAM neurons (Fig. 1c,

137 d). Therefore, *Lrrk* gain of function causes not only developmental loss but also age-
138 dependent loss of PAM neurons. Remarkably, overexpression of *Fer2* in PAM neurons
139 prevented the reduction of TH-positive cell counts induced by the expression of wild-type or
140 mutant *Lrrk* (Fig. 1a, b). The analysis of cell counts using RedStinger found that PAM
141 neuron loss caused by the mutant *Lrrk*, but not the WT *Lrrk*, was rescued with *Fer2*
142 overexpression at least partially (Fig. 1c, d). Forced expression of *Lrrk* in $Fer2^{2}$ heterozygous
143 background resulted in PAM neuron loss to a similar extent as in wild-type background
144 (Supplementary Fig. 1b). *Lrrk* overexpression in $Fer2^{2}$ homozygous mutants additively
145 enhanced PAM neuron loss compared with either of the single genetic perturbations
146 (Supplementary Fig. 1b). These results suggest that *Fer2* and *Lrrk* act in independent
147 pathways but *Fer2* overexpression can attenuate *Lrrk*-induced neuronal damage.
148 Mutations in the *PRKN* gene, which encodes the E3 ubiquitin ligase Parkin, are linked
149 to autosomal recessive juvenile PD[37]. *Drosophila parkin* loss-of-function mutant $park^{1}$
150 exhibits PD-like phenotypes, including locomotor deficits, mitochondrial impairments and
151 loss or shrinkage of a few subclasses of DA neurons[38,39]. Since the effect of *parkin* loss of
152 function on the integrity of DA neurons in the PAM cluster has not been evaluated in
153 previous studies, we visualized PAM neurons using anti-TH immunostaining and targeted
154 expression of RedStinger in $park^{1}$ mutants. An age-dependent reduction in the number of TH-
155 positive PAM neurons was observed in $park^{1}$ homozygotes (Supplementary Fig. 1c).
156 However, the number of cells expressing RedStinger with the PAM neuron driver was not
157 significantly different between the heterozygous and homozygous $park^{1}$ mutants
158 (Supplementary Fig 1d). Therefore, $park^{1}$ mutation reduces TH expression in PAM neurons,
159 which likely leads to functional impairments, although it does not cause cell loss.
160 Parkin mutations lead to severe defects in mitochondrial morphology and function in
161 all organisms studied thus far, including flies[40–43]. We therefore examined whether *Fer2*

162 overexpression ameliorates mitochondrial morphology in DA neurons of *park*^{1} flies by
163 expressing mitochondria-targeted GFP (mitoGFP) in PAM neurons. In contrast to the
164 reticular mitochondria observed in control flies, the majority of mitochondria appeared more
165 rounded in PAM neurons of *park*^{1} mutants (Fig. 1e). This observation was quantitatively
166 confirmed by the analysis of mitochondria circularity, which showed a shift towards more
167 globular mitochondria in *park*^{1} compared with control (*park*^{1}/+) flies (Fig. 1f). Remarkably,
168 the overexpression of *Fer2* in PAM neurons restored tubular mitochondrial morphology in
169 *park*^{1} flies (Fig. 1e, f). Furthermore, to determine if *Fer2* overexpression improves the
170 functioning of mitochondria in *park*^{1} flies, we assessed mitochondrial membrane potential in
171 PAM neurons using the tetramethylrhodamine methyl ester (TMRM) staining. TMRM
172 fluorescence levels were significantly reduced in homozygous *park*^{1} mutants compared to
173 *w*^{1118}, indicating the decrease in mitochondrial membrane potential as a result of *parkin* loss
174 of function. Overexpression of *Fer2* increased TMRM fluorescence to the levels equivalent
175 to those in *w*^{1118} and *park*^{1}/+ flies (Fig. 1g). These results indicate that *Fer2* can counteract
176 both morphological and functional impairments in mitochondria caused by loss of *parkin*.
177 The findings that *Fer2* overexpression cell-autonomously prevents cellular and
178 mitochondrial damage in the PAM cluster DA neurons in two independent familial PD
179 models suggest that *Fer2* gain of function might confer dopaminergic neuroprotection against
180 a broad spectrum of genetic and chemical insults. We therefore tested if *Fer2* overexpression
181 can protect DA neurons from damage caused by oxidative stress, using an assay in which
182 flies were exposed to a non-lethal dose of hydrogen peroxide (H_2O_2). 7-day-old flies were fed
183 with 5% H_2O_2 for 24h, and 7 days later DA neurons in the brains were examined by anti-TH
184 immunostaining. Whereas this treatment does not immediately affect PAM neuron integrity
185 in control flies[28,29], 7 days later it triggered the loss of approximately 10% of DA neurons in
186 the PAM cluster in *w*^{1118} flies, *Fer2*^{2}/+ flies and flies carrying a PAM-specific driver (Fig.

187 2a). The PAM neuron loss was exacerbated in flies homozygous for the *Fer2*^{2} allele,
188 consistent with our previous finding that *Fer2* inactivation renders PAM neurons more
189 vulnerable to oxidative stress[28,29]. In contrast, *Fer2* overexpression in PAM neurons
190 prevented H_2O_2-induced PAM neuron loss (Fig. 2a). These results indicate that *Fer2* gain of
191 function protects DA neurons in the PAM cluster from oxidative insults.
192 ROS production increases as flies age[44]. Interestingly, we found an age-dependent
193 increase in FER2 protein levels in PAM neurons, parallel to the augmentation of ROS levels
194 in the brain (Fig. 2b-e). Combined with the fact that *Fer2* loss of function causes a
195 progressive loss of PAM neurons, this finding suggests that FER2 is upregulated to protect
196 PAM neurons from age-dependent increases in endogenous oxidative stress. Taken together,
197 these results provide evidence that *Fer2* is a potent neuroprotective transcription factor for
198 PAM dopaminergic neurons, counteracting various genetic and oxidative insults.
199
200 **Identification of *Fer2* direct targets by a combination of ChIP-seq and RNA-seq**
201 **approaches**
202 To investigate how *Fer2* elicits dopaminergic neuroprotection, we wished to identify *Fer2*
203 transcriptional targets. To this end, we first determined the genome-wide binding sites of
204 FER2 using chromatin immunoprecipitation coupled to sequencing (ChIP-seq). Since FER2-
205 specific antibodies were unattainable, ChIP-seq was performed on the heads of 14-day-old
206 flies harboring a *Fer2::GFP::V5* genomic transgene in *Fer2*^{1} mutant background[28], using
207 anti-V5 antibody (Fig. 3a). *Fer2::GFP::V5* recapitulates the physiological dosage and
208 expression pattern of *Fer2*, as it is expressed in PAM neurons but scarcely in other cells in
209 the brain (Supplementary Fig. 2a), in agreement with existing single-cell RNA-seq data[45,46].
210 We also found that *Fer2::GFP::V5* rescues PAM neuron loss and locomotor defects in *Fer2*^{1}
211 mutants, verifying that FER2::GFP fusion protein retains the function of FER2

212 (Supplementary Fig. 2b, c). We identified 269 FER2-bound regions, which were annotated to
213 279 putative *Fer2* target genes (Supplementary Data 1). FER2-bound sequences were highly
214 enriched with a 12-nucleotide motif containing a canonical bHLH binding site (CANNTG),
215 validating the specificity of the procedure (Fig. 3b).

216 The binding of transcription factors to chromatin does not necessarily lead to
217 transcriptional regulation of nearby genes[47]. To determine which binding events regulate
218 proximal gene expression, we next identified transcripts that are up- or downregulated after a
219 transient overexpression of *Fer2* and compared these transcripts with the ChIP-seq data. The
220 heat-inducible *hs-GAL4* was used to ubiquitously but acutely express *Fer2,* and RNA-seq
221 was performed on fly heads collected 12 and 48 h after a 3-h heat shock. The same heat-
222 shock treatment was applied to the flies carrying *hs-GAL4* but not *UAS-Fer2* to identify and
223 exclude from our analysis any heat-responsive gene (Fig. 3c). These experiments identified
224 328 genes (12 h after heat shock) and 916 genes (48 h after heat shock) differentially
225 expressed in the head following *Fer2* overexpression (Fig. 3c and Supplementary Data 2).
226 Then, by comparing the head RNA-seq and *Fer2* ChIP-seq data, we found 32 genes that were
227 present in FER2 ChIP-seq and also differentially expressed 48 h after *Fer2* overexpression
228 (Fig. 4b). These genes are considered as potential *Fer2* transcriptional targets. The overlap
229 was statistically highly significant (hypergeometric probability = 0.0004). In contrast, there
230 was no statistically significant overlap between the ChIP-seq data and the genes differentially
231 expressed 12 h after heat-shock, therefore we focused our subsequent analysis on the data set
232 obtained at the 48 h timepoint. The ChIP-seq profiles and RNA-seq data of two *Fer2* targets,
233 *CG8128* and *skd*, are presented as examples in Fig. 3d. Because *Fer2* expression is largely
234 restricted to PAM neurons, the majority of FER2 ChIP signal represents FER2 binding within
235 PAM neurons, whereas whole-head RNA-seq following *Fer2* induction detects genes also
236 expressed outside the PAM cluster. Therefore, to determine whether the *Fer2* targets

237 identified above are expressed in PAM neurons, we profiled the transcriptome of isolated
238 PAM neurons (Fig. 4a). Indeed, the majority (26 out of 32) of *Fer2* target genes identified by
239 the ChIP-seq/head RNA-seq intersectional analysis were found to be expressed in PAM
240 neurons (Fig. 4b), validating this subset of 26 genes as *bona fide* direct transcriptional targets
241 of *Fer2* (Fig. 4c, Supplementary Data 3).

242 A further analysis of the 26 *bona fide* targets revealed that *Fer2* preferentially binds to
243 introns of the target genes and acts as a repressor in most instances, as the majority of direct
244 targets are downregulated after acute *Fer2* overexpression (Fig. 4d, e). A large fraction of the
245 26 *Fer2* direct targets are involved in the regulation of gene expression, including
246 transcription factors (*ftz-f1*, *Eip75B*, *Eip93F*, and *Snoo*), transcriptional coregulators (*skd*),
247 components of chromatin remodeling complexes (*Smr*, *osa*, and *sba*) and histone modifiers
248 (*gpp*). These genes show a significant interconnectivity (p-value = 0.00006) either physically
249 or functionally, as inferred from STRING database analysis, suggesting that they may
250 cooperate to regulate downstream gene expression (Fig. 4c).

251

252 **Multiple *Fer2* direct target genes contribute to the maintenance of PAM dopaminergic**
253 **neurons**

254 Next, we assessed whether *Fer2* direct target genes have roles similar to *Fer2* by
255 manipulating their expression levels individually in PAM neurons and monitoring neuronal
256 survival. To mimic the effect of *Fer2* loss of function, target genes upregulated by *Fer2* were
257 knocked-down via RNAi, and genes downregulated by *Fer2* were overexpressed in PAM
258 neurons. PAM neurons were examined at the age of 35 days with anti-TH staining. 17 out of
259 26 *Fer2* direct targets were tested in this assay, since transgenic lines for RNAi or
260 overexpression for 7 genes were unavailable or lethal when combined with the *Fer2-GAL4*
261 driver and two other genes, *CG1578* and *Theg*, could not be efficiently downregulated with

262 available *UAS-RNAi* lines (approximately 30% downregulation assessed by RT-qPCR). Of
263 note, driving *UAS-CG4998 RNAi* with the ubiquitously expressing *tubulin-GAL4* or *actin-*
264 *GAL4* was lethal, which suggests a high efficacy of the UAS-RNAi line for *CG4998*. The fly
265 lines used in this assay are described in Supplementary Data 3 along with their references.
266 Genetic manipulation of one third of the tested genes (6 out of 17) caused a significant loss of
267 PAM neurons compared with the driver-only control, thus partially recapitulating the
268 phenotype of *Fer2* loss of function (Fig. 4f and Supplementary Data 3). These results broadly
269 confirm that the ChIP-seq and RNA-seq intersectional analysis identified a panel of *Fer2*
270 direct targets that contribute to the role of *Fer2* in the development and maintenance of PAM
271 neurons.
272
273 ***Fer2* is a master regulator of mitochondrial health and function**
274 Since many *Fer2* direct targets are transcriptional regulators, *Fer2* most likely orchestrates
275 the expression of a larger set of secondary targets to promote the survival of PAM neurons.
276 To decipher downstream biological processes controlled by *Fer2*, we also profiled the
277 transcriptome of isolated PAM neurons following PAM-specific, constitutive *Fer2*
278 overexpression (Fig. 4a). We reasoned that this approach should capture the long-term
279 consequences of *Fer2* overexpression on gene expression in PAM neurons. A comparison of
280 PAM neuron transcriptomes of flies overexpressing *Fer2* and age-matched controls identified
281 132 differentially expressed genes (DEGs) (24 genes upregulated and 108 genes
282 downregulated; $p<0.01$). These genes were distinct from the 26 direct targets and were
283 considered as *Fer2* secondary targets (Fig. 4a, b; Supplementary Data 4).
284 Gene ontology (GO) analysis of *Fer2* secondary targets revealed a marked enrichment
285 of nuclear-encoded mitochondrial genes among up-regulated genes. Down-regulated genes
286 are enriched with the GO terms “translational termination” and “vacuoles” (Fig. 4g). Up-

287 regulated mitochondrial genes include a component of the electron transport chain (ETC)
288 (*ND-15*), genes involved in the assembly or maturation of ETC complexes (*Sdhaf3*, *CG7639*,
289 *Cchl*, *CG5037*), and the mitochondrial *Superoxide dismutase 2* (*Sod2*) (Fig. 4g and
290 Supplementary Data 4.). As a crucial player in the cellular antioxidant response, SOD2 is
291 localized to the mitochondrial matrix and catalyzes superoxide ($O_2\bullet^-$) to the less reactive
292 H_2O_2[48]. Remarkably, *Sod2* overexpression in PAM neurons partially but significantly
293 prevented neuronal loss in *Fer2*[2] mutant flies, which suggests that *Sod2* acts downstream of
294 *Fer2* to contribute to dopaminergic neuroprotection (Fig. 4h). Combined with the finding that
295 *Fer2* regulates the expression of numerous mitochondrial genes, these results demonstrate
296 that *Fer2* plays a prominent role in the maintenance of mitochondria.
297 To explore how *Fer2* direct targets control a large set of secondary targets, we
298 searched for transcription factor binding sites that are significantly overrepresented in the
299 promoters of DEGs in PAM RNA-seq. Seven binding motifs were found to be enriched,
300 including those for Broad, Dichate and USP, which are expressed in PAM neurons.
301 Interestingly, these genes are known to form complexes or functionally interact with FTZ-F1,
302 a *Fer2* direct target[49,50] (STRING database, https://string-db.org/) (Supplementary Fig. 3a, b).
303 Consistent with the finding that *ftz-f1* is downregulated by FER2, *ftz-f1* overexpression leads
304 to the loss of PAM neurons (Fig. 4f). Therefore, gene regulatory networks that control PAM
305 neuron maintenance initiated by *Fer2* may be mediated by FTZ-F1 together with these
306 factors. Another *Fer2* direct target, SMRTR, can interact with USP[51], and may thus initiate a
307 second pathway to control gene networks in PAM neurons (Supplementary Fig. 3a, b).
308
309 **Conditional deletion of *Nato3* in differentiated DA neurons leads to locomotor deficits in**
310 **aged mice**

311 Since *Fer2* is required for the maintenance of mitochondrial health and integrity in DA
312 neurons, we wondered whether the mammalian homolog of *Fer2* has a similar role. Blast
313 searches found four mammalian bHLH transcription factors with a significant similarity to
314 FER2, namely P48/PTF1A, NATO3 (N-TWIST, FERD3L), TCF15, and TWIST1 (Fig. 5a).
315 Interestingly, it has been shown that *Nato3* is expressed in the progenitors of mDA neurons
316 and is required for dopaminergic neurogenesis[32,33,52], analogously to the role of *Fer2* in the
317 genesis of DA neurons in flies[28]. Furthermore, RNA-seq data from the Genotype-Tissue
318 Expression (GTEx) project (the GTEx Consortium, Nat Genetics, 2013)[53] indicate that,
319 among human tissues, *NATO3* expression is relatively restricted to the SN of the adult brain
320 (Fig. 5b), whereas the other three *Fer2* homologs show little or no expression in the SN
321 (Supplementary Fig. 4). Based upon these evident similarities in the protein sequence, the
322 expression in mDA neurons and the role in the development of mDA neurons, we consider
323 *Nato3* to be a functional homolog of *Fer2*.
324 To investigate whether *Nato3* is involved in the maintenance of postnatal mDA
325 neurons, we first determined its expression levels and specificity in the mouse brain. Reverse
326 Transcription quantitative PCR (RT-qPCR) analysis of dissected brain regions displayed a
327 significant enrichment of *Nato3* transcripts in the midbrain of 4-month-old mice (Fig. 5c).
328 *Nato3* continues to be expressed at similar levels in the midbrain of young (1-month-old),
329 adult (4-month-old) and aged (14-month-old) mice (Fig. 5d). *In situ* hybridization combined
330 with anti-TH immunostaining showed *Nato3* mRNA expression in the DA neurons of the SN
331 and the ventral tegmental area (VTA) of 14-month-old mice. *Nato3* expression was also
332 detected in non-TH-positive cells in the SN and VTA (Fig. 5e).
333 Having verified the expression of *Nato3* in adult mDA neurons, we sought to
334 conditionally delete *Nato3* in postmitotic DA neurons and investigate its consequences to
335 dopamine-related behavior and the integrity of mDA neurons. We generated a mouse strain

336 bearing the *loxP*-flanked (floxed) allele of *Nato3* and crossed it with the *DAT-Cre* transgenic
337 mouse expressing the Cre recombinase under the control of the dopamine transporter gene
338 (*Slc6a3*) regulatory sequences[54]. *DAT-Cre* expression is known to arise postnatally in
339 differentiated midbrain DA neurons, has no deleterious effects on DA neurons, and does not
340 alter locomotion or anxiety-related behaviors[54,55]. We obtained homozygous *Nato3*-floxed
341 animals harboring either no copies ($Nato3^{floxed}$, referred to as control) or one copy of the
342 *DAT-Cre* transgene ($Nato3^{DAT\text{-}Cre}$, referred to as *Nato3* cKO) (Fig. 6a). RT-qPCR analysis
343 showed approximately 50% reduction of *Nato3* expression in the ventral midbrain in
344 $Nato3^{DAT\text{-}Cre}$ mice compared to controls (Fig. 6b). *In situ* hybridization revealed the reduction
345 of the percentage of TH^+ neurons expressing *Nato3* mRNA from ~90% to ~23% in *Nato3*
346 cKO (Fig. 6c, d), which confirms the high efficiency of *DAT-Cre* mediated *Nato3* ablation in
347 mDA neurons.

348 We analyzed control and *Nato3* cKO mice at different ages using assays for
349 dopamine-related behaviors. In the pole test, which is a sensitive assay for motor impairment
350 associated with reduced striatal dopamine in rodents[56], *Nato3* cKO mice took significantly
351 longer to turn and descend the pole than control mice at 13 months, while no difference was
352 observed in younger animals (Fig. 6e). This observation indicates an age-dependent decline
353 in motor coordination in *Nato3* cKO mice. Spontaneous activity levels measured via
354 voluntary wheel running over three days were similar between *Nato3* cKO and control mice
355 until 13 months of age. However, the activity levels of *Nato3* cKO significantly declined at
356 16 months (Fig. 6f). In contrast, no differences were found between *Nato3* cKO and control
357 mice in the open field test, which measures exploratory behavior when mice are placed in a
358 novel environment[57] (Supplementary Fig. 5). These results indicate that *Nato3* ablation in
359 postmitotic DA neurons lead to motor abnormalities in aged mice, possibly caused by an age-
360 dependent decline in the nigrostriatal dopaminergic function.

361

362 ***Nato3* is required for the maintenance of mitochondrial integrity in midbrain DA**

363 **neurons**

364 To broadly assess the integrity of the nigrostriatal pathway, ventral midbrain and striatal

365 sections of 16- to 18-month-old mice were analyzed by anti-TH immunohistochemistry. The

366 number of DA neuron cell bodies in the SN and VTA (Fig. 6g, h), as well as the density of

367 TH^+ fibers in the striatum (Fig. 6i, j), did not show significant differences between control

368 and *Nato3* cKO mice. Analysis of extracellular DA levels in the striatum of 16- to 18-month-

369 old mice by *in vivo* microdialysis found no difference between control and *Nato3* cKO mice

370 (Fig. 6k). Therefore, locomotor deficits in the *Nato3* cKO mice likely originate from

371 functional impairments of DA neurons, such as changes in electrophysiological properties,

372 rather than an overt loss of cellular integrity.

373 *Fer2* mutation impairs mitochondrial morphology selectively in the PAM cluster DA

374 neurons, which precedes the degeneration of PAM neurons and locomotor deficits in

375 *Drosophila*[28]. To determine whether *Nato3* ablation also leads to mitochondrial abnormalities

376 in DA neurons in mice, we first visualized mitochondria in the SN using the antibodies

377 against mitochondrial cytochrome c oxidase subunit 4 (COX4). The mitochondria appeared

378 more globular in DA neurons of the SN in aged (16-18 months old) *Nato3* cKO mice

379 compared with age-matched controls (Fig. 7a). Quantification of mitochondrial circularity

380 showed a statistically significant increase (i.e. an accumulation of rounder mitochondria) in

381 *Nato3*-ablated DA neurons, confirming the visual impression (Fig. 7b). We further examined

382 the ultrastructure and morphology of mitochondria in the SN of 6-month-old and 16~18-

383 month-old mice using transmission electron microscopy. In TH-labeled neurons of control

384 mice at both ages, most mitochondria (>88%) appeared normal, showing a dense and uniform

385 matrix and regularly distributed cristae (Fig. 7c, top panels, and Fig. 7d). Strikingly, whereas

386 most mitochondria were normal in 6-month-old *Nato3* cKO mice, a large fraction (46%) of
387 mitochondria from the aged *Nato3* cKO mice displayed an aberrant morphology, showing a
388 reduced and patchy matrix density with few remaining cristae; in certain cases these
389 mitochondria contained almost no cristae, presented white inclusions and appeared
390 dysmorphic (Fig. 7c bottom panels and 7d). Mitochondria from TH-negative cells appeared
391 normal in aged *Nato3* cKO mice, suggesting that the age-dependent deterioration of
392 mitochondrial morphology was cell-autonomously induced by *Nato3* deletion in DA neurons
393 (Fig. 7c right bottom panel). Although mitochondrial size did not differ between the two
394 genotypes at both ages, mitochondria in the SN neurons in aged *Nato3* cKO mice were
395 rounder than those in the control mice (Fig. 7e). These results demonstrate that *Nato3* is
396 required for the maintenance of mitochondrial integrity in the DA neurons of the SN.
397 Since *Fer2* loss of function downregulates SOD2 and SOD2 overexpression partially
398 rescues the loss of PAM neurons in *Fer2*^{2} *Drosophila* mutants (Fig. 4h), we wondered
399 whether SOD2 is downregulated in *Nato3* cKO mice. Anti-SOD2 immunostaining indeed
400 found a significant reduction in SOD2 levels in DA neurons in the VTA and SN of old *Nato3*
401 cKO mice (Fig. 7f, g). This observation suggests a conserved mechanism underlying the role
402 of *Fer2* and *Nato3* in maintaining mitochondrial integrity. Several transcription factors
403 involved in mDA neuron development are neuroprotective in postmitotic mDA neurons in
404 the adult brain[16]. Therefore, to explore the molecular mechanism linking *Nato3* ablation and
405 mitochondrial dysfunction in mDA neurons, we analyzed the expression levels of a panel of
406 neuroprotective "developmental" transcription factors in the vMB by RT-qPCR.
407 Interestingly, *Engrailed 1* (*En1*) was significantly downregulated in *Nato3* cKO mice. *Lmx1b*
408 mRNA levels were also reduced in *Nato3* cKO compared to control, but the difference did
409 not narrowly reach statistical significance (p=0.0571) (Fig. 7h). *En1* regulates expression of
410 key proteins of mitochondrial complex I in mDA neurons[20], and *Lmx1b* is required for

411 autophagic-lysosomal pathway[9] and mitochondrial functions[10]. Taken together, our results
412 suggest the possibility that *Nato3* regulates the expression of neuroprotective transcription
413 factors, through which it controls mitochondrial function and morphology in mDA neurons.
414

415 **DISCUSSION**

416 Our results demonstrate that *Fer2* is a master regulator of a transcriptional network that
417 maintains mitochondrial integrity in DA neurons in *Drosophila*. This property renders *Fer2* a
418 potent dopaminergic neuroprotective factor against genetic and oxidative insults implicated
419 in PD pathogenesis. Furthermore, we show that *Nato3*, a mammalian homolog of *Fer2*, is
420 required for the maintenance of mitochondrial integrity in mDA neurons. Both *Fer2* and
421 *Nato3* are developmental transcription factors for DA neurons that continue to be expressed
422 throughout life, and their loss of function in differentiated DA neurons leads to locomotor
423 deficits in aged animals. Our findings corroborate the critical role of developmental
424 transcription factors in the lifelong maintenance of DA neurons and suggest the evolutionary
425 conservation of transcriptional mechanisms for dopaminergic neuroprotection and
426 mitochondrial integrity.

427 *Drosophila Fer2* (*48 related 2*, CG5952) and its paralogs *Fer1* and *Fer3* were
428 originally named for their similarity to the p48 subunit of the pancreas transcription factor 1
429 complex (PTF1) in the bHLH domain by the group of Yuh Nung Jan[58]. Independently, due to
430 the similarity to mammalian Atonal within the bHLH domain, *Fer3* (CG6913) was named
431 *Drosophila Nephew of Atonal 3* (*Dnato3*) by the group of Nissim Ben-Arie[59]. Ben-Arie's
432 group also isolated a mouse homolog of *Dnato3* and named it *MNato3*[59]. Brian L Black's lab
433 also independently isolated the same mouse gene and named it *Neuronal-twist* (*N-twist*), due
434 to its high sequence similarly to *M-twist*[60]. It is puzzling that, whereas Jan's group has
435 reported the expression of *Fer2* mRNA in the brain and ventral nerve cord (VNC) of the

436 embryo and *Fer3* expression in the primordial midgut of the embryo[58], Ben-Arie's and
437 Black's groups have shown the expression of *Fer3* mRNA in the CNS of the embryo, which
438 supports the idea that *Fer3* is the homolog of *Nato3*[60]. Notwithstanding this inconsistency, we
439 argue that *Fer2* is a functional homolog of *Nato3* based on the following reasons. The fact
440 that fewer DA neurons are generated in *Fer2* loss-of-function mutants[28] is strikingly similar
441 to the observation that 30% fewer mDA neurons are formed in *Nato3* constitutive KO[32],
442 suggesting that *Fer2* bears a proneural function similar to that of *Nato3*. FER2 bHLH domain
443 shows a high similarity to that of NATO3 as well as to FER1 and FER3 (Supplementary Fig.
444 4a). Moreover, we have demonstrated here and in previous work[28] that DA neurons are the
445 primary site of *Fer2* expression and function, and that both *Fer2* and *Nato3* are required for
446 mitochondrial maintenance in differentiated DA neurons. Nevertheless, the possibility that
447 *Fer3* may also have similar roles as *Fer2* in the development and maintenance of DA neurons
448 cannot be excluded and is worthy of further investigation.
449 This study is the first to report the function of *Nato3* in differentiated mDA neurons in
450 mice. *Nato3* is classically known as a neurogenic transcription factor, expressed in the floor
451 plate cells in the developing mesencephalon and spinal cord[32,34]. Although *Nato3* expression
452 in the spinal cord of postnatal and adult mice has been reported[61], we found here its presence
453 in the mDA neurons of adult mice. By conditionally ablating *Nato3* in postmitotic DA
454 neurons, we were able to distinguish the function of *Nato3* in mature mDA neurons, i.e. the
455 maintenance of mitochondrial integrity, from its role in neurogenesis. Importantly, human
456 *Nato3* is expressed almost exclusively in the SN among adult tissues (Fig. 5b) (the GTEx
457 Consortium, Nat Genetics, 2013)[53]. Thus, it is plausible that human *Nato3* also plays an
458 important role in the mitochondrial maintenance in SN dopaminergic neurons.
459 The genesis, specification and differentiation of mDA neurons are governed by a
460 complex web of transcription factors[62]. Whereas *Nato3* acts as an "early transcription factor"

461 required for neurogenesis[32], it can also directly regulate *Lmx1b*, *Shh* and *Foxa2* and thereby
462 indirectly regulates the "late transcription factor" *Nurr1*[33,52]. Since *Lmx1b*, *Foxa2* and *Nurr1*
463 are neuroprotective transcription factors[9,12,13,19], *Nato3* might contribute to dopaminergic
464 neuroprotection by regulating some of these genes. Indeed, we find here that *En1* and *Lmx1b*
465 are downregulated in the vMB of *Nato3* cKO mice, supporting this possibility. Furthermore,
466 a recent study has shown that *Nato3* is a potential target of the transcription factor sterol
467 regulatory element binding protein 1 (SREBP1), a key player of mDA neurogenesis[63].
468 SREBP1 also upregulates *Foxa2*[63], which in turn positively regulates *Nato3* expression
469 during development[64]. Importantly, a polymorphism in the *Srebf1* gene encoding SREBP1 is
470 linked to PD[65,66]. Therefore, the evidence is growing that gene regulatory programs involving
471 DA developmental genes, including *Nato3*, have important roles in the survival of mDA
472 neurons during aging and offer an opportunity to study PD.
473 Identification of *Nato3* transcriptional targets and downstream molecular events in
474 differentiated mDA neurons will provide crucial information to understand the role of *Nato3*
475 in mitochondrial maintenance. While further studies are required to obtain such data, here we
476 have performed homologous experiments in *Drosophila*, i.e. identification of direct and
477 indirect targets of *Fer2* in DA neurons in the PAM cluster. An intersectional approach
478 combining ChIP-seq, whole-head RNA-seq and RNA-seq of isolated PAM neurons,
479 unequivocally identified 26 direct and over 100 indirect *Fer2* target genes expressed in PAM
480 neurons. Among *Fer2* indirect targets, genes involved in mitochondrial function and
481 structure, including those required for ETC complexes assembly, are remarkably enriched.
482 Malfunction of the ETC leads to ROS overproduction, which in turn induces mitochondrial
483 DNA mutations, alters membrane permeability and mitochondria morphology, and further
484 damages the ETC complexes, in a pathogenic self-reinforcing loop. Indeed, dysfunctions of
485 the ETC, particularly of Complex I, have been proposed as a leading mechanism of DA

486 neurodegeneration[67,68]. Thus, our molecular data are in accordance with the observation that
487 *Fer2*^{2} flies display an overt defect in mitochondrial networks[28].
488 It is noteworthy that *Sod2*, which encodes mitochondrial superoxide dismutase, is also
489 an indirect target of *Fer2*. Consistent with this finding, *Sod2* overexpression partially rescues
490 the loss of PAM neurons in *Fer2*^{2} mutants. Furthermore, *Fer2* overexpression reverses
491 mitochondrial abnormalities in the PAM neurons of *park*^{1} mutants and prevents PAM neuron
492 loss in genetic and toxin models of PD. These results are in agreement with previous reports
493 that *Sod2* and *Sod2*-mimetic agents are protective in cell and fly models of PD[69], and endorse
494 the further exploration of *Sod2* as a potential therapeutic target for PD. Interestingly, SOD2
495 levels are reduced in the mDA neurons of *Nato3* cKO mice, suggesting that neuroprotective
496 mechanisms regulated by *Fer2* in flies and *Nato3* in mice are at least partly conserved.
497 Among *Fer2* direct targets, we found six genes whose dysregulation induces a loss of
498 PAM neurons. None of these genes have been previously related to the DA system or
499 implicated in neuronal development or survival. Further studies are needed to clarify how
500 these novel actors and their mammalian homologues contribute to the biology of DA
501 neurons. The number of new genes implicated in PAM neuron survival may increase in the
502 future, as our list of *Fer2* direct targets is likely not exhaustive. *Fer2* is a stress-responsive
503 transcription factor that is upregulated by oxidative insult or possibly by other stressors[28].
504 Under such conditions FER2 may be recruited to and/or regulate different sets of target
505 genes.
506 A large fraction of *Fer2* primary targets encode transcription factors or chromatin
507 proteins. This positions *Fer2* at the vertex of multiple transcriptional cascades and suggests
508 that *Fer2* orchestrates the expression of a broad set of secondary targets (Supplementary Fig.
509 3b). *Fer2* expression is restricted to PAM neurons and a few other cell clusters in the brain,
510 and ubiquitous or even pan-neuronal constitutive overexpression of *Fer2* causes lethality

511 (data not shown), indicating that genetic programs driven by *Fer2* are highly specific to PAM
512 neurons.

513 PD progresses from the asymptomatic (preclinical) period to a stage with a variety of
514 nonmotor symptoms and subtle motor impairments that do not meet diagnostic criteria
515 (prodromal PD), before a definite diagnosis is reached[70]. Modeling in animals this latent
516 phase of the disease would facilitate the development of disease-modifying therapies and the
517 discovery of early PD biomarkers. *Nato3* cKO mice reproduce some features of prodromal
518 PD, presenting moderate motor deficits and quasi-normal mDA neurons that accumulate
519 abnormal mitochondria. Striatal extracellular DA concentration in *Nato3* cKO mice are not
520 significantly different from that of control mice at 16-18 months, when *Nato3* cKO mice
521 manifest locomotor deficits. This further suggests that functional impairments in DA neurons,
522 such as changes in electrophysiological properties[71] or in monoamine metabolism[72], might
523 account for motor deficits in *Nato3* cKO mice. Likewise, other PD mouse models, such as
524 *PINK1* deficiency and *Parkin* deletion mice, do not show loss of DA neurons or reduction in
525 nigrostriatal DA release, while exhibiting mitochondrial impairments and locomotor
526 phenotypes[37,72]. There is growing evidence that neurodegeneration in PD is manifested after
527 several risk factors, including genetic predisposition, toxin exposure and aging, interact to
528 overcome protective compensatory mechanisms[73]. Future work is needed to determine
529 whether exposing *Nato3* cKO mice to a second genetic or environmental insult exacerbates
530 its PD-related phenotypes and trigger overt DA neurodegeneration.

531 The activation of neuroprotective transcription factors offers potent therapeutic
532 opportunities, allowing to modulate multiple downstream pathways in parallel. Indeed, *Nurr1*
533 and *Foxa2* gene delivery[19], *Nurr1* activators[74] and *En1* infusion[20] in rodent PD models have
534 shown encouraging results. In light of our findings that *Fer2* confers neuroprotection in
535 multiple fly PD models, it is tempting to speculate that the overexpression or activation of

536 *Nato3* may protect mDA neurons from genetic and environmental insults in mammals, with
537 potential far-reaching implications for PD treatment.
538
539 **METHODS**
540 ***Drosophila* stocks and maintenance**
541 The following lines were obtained from the Bloomington *Drosophila* Stock Center (BDSC)
542 (Indiana University, Bloomington, IN): *UAS-RedStinger* (#8546), *UAS-Sod2* (#24494), *park*^{1}
543 (#34747), and *hs-GAL4* (#1799). *Fer2::GFP::V5*, *PBac{RB}Fer2*^{e03248} (referred to as *Fer2*^{1}),
544 *Mi{ET1}Fer2*^{MB09480} (referred to as *Fer2*^{2}), *Fer2-GAL4, R58E02-GAL4*, *UAS-mitoGFP*, and
545 *UAS-Fer2::FLAG* lines were previously described[26,28,75]. *UAS-Lrrk WT* and *UAS-Lrrk*
546 *I1915T* were a kind gift from Yuzuru Imai[76]. All of the lines used to overexpress or knock-
547 down *Fer2* primary targets are described in the Supplementary Data 3. All flies were
548 maintained on standard cornmeal-agar food at 25 °C in a 12 h:12 h light-dark cycle and under
549 controlled humidity.
550
551 **Fly brain immunohistochemistry**
552 Immunostaining of whole fly brains was performed as previously described[28]. Briefly, the
553 flies were decapitated, and the heads were fixed in 4% paraformaldehyde (PFA) + 0.3%
554 Triton X-100 for 1 h on ice and washed three times with PBST-0.3 (PBS, 0.3% Triton X-
555 100). The cuticle was partially removed, and the partly opened heads were incubated with
556 blocking solution (5% normal goat serum, PBS, 0.3% Triton X-100) for 1 h at room
557 temperature (RT) on a rocking platform. Subsequently, the samples were incubated with
558 primary antibodies for 48 h at 4 °C. After three 20 min washes with PBST-0.3, the samples
559 were then incubated with Alexa Fluor-conjugated secondary antibodies overnight at 4 °C.
560 After three 20 min washes with PBST-0.3, the remaining cuticle and trachea were removed,

561 and the brains were mounted in Vectashield medium (Vector Laboratories). Primary
562 antibodies and the dilution factors were as follows: rabbit polyclonal anti-TH (ab152,
563 Millipore) 1:100, polyclonal rabbit anti-GFP (A6455, Invitrogen) 1:250. Neuropil was
564 counterstained with the mouse monoclonal antibody nc82 (Developmental Studies
565 Hybridoma Bank) 1:100 to visualize the entire brain and assess its integrity. Secondary
566 antibodies and the dilution factors were as follows: goat anti-rabbit IgG Alexa Fluor 488
567 conjugate (A-11034, Thermo Fisher Scientific) 1:250, goat anti-mouse IgG Alexa Fluor 633
568 conjugate (A-21052, Thermo Fisher Scientific) 1:250.
569
570 **Mouse brain immunohistochemistry**
571 Animals were anesthetized and perfused through the left ventricle with 0,2% Heparin in PBS
572 at RT followed by ice-cold 10% formalin solution (Sigma HT501128-4L). The brains were
573 dissected and post-fixed for 72 h in fresh 4% PFA (Thermo Fisher Scientific #28906) before
574 being embedded in low melting point agarose (Thermo Fisher Scientific #R0801) and
575 sectioned in a sliding vibratome at a thickness of 40 µm. Striatum sections were stained as
576 floating sections. Ventral midbrain sections were adhered to the SuperFrost plus slides
577 (Thermo Fisher Scientific J1800AMNZ) before staining. Slices were incubated in blocking
578 buffer (4% non-fat milk, 4% Bovine Serum Albumin (BSA), PBS) containing 0,1% Triton X-
579 100 for 30 min at RT. The sections were then incubated with primary antibodies in blocking
580 buffer containing 0,1% Tween for 48 h at 4 °C. After three 30 min washes in washing buffer
581 (0.1% Tween, PBS), sections were incubated with the corresponding secondary antibody
582 overnight at 4 °C, in the dark. After three 30 min washes in washing buffer, the slices were
583 mounted with DABCO-glycerol mounting medium (25 mg/ml DABCO (Sigma D27802-
584 25G), 90% glycerol, PBS; pH 8,6). For nuclear staining, prior to mounting midbrain slices
585 were treated with 100µg/ml RNAse A (#EN0531, Thermo Fisher Scientific) for 30 min at

586 37 °C, and then incubated with TO-PRO-3 iodide (T3605, Sigma) for 30 min at RT. Primary
587 antibodies and dilution factors were as follows: rabbit polyclonal anti-TH (Millipore ab152)
588 1:300, mouse anti-TH (Immunostar 22941) 1:300, mouse anti-COX4 (Thermo Fisher
589 Scientific 1D6E1A8) 1:300, rabbit anti-SOD2 (abcam ab13534). Secondary antibodies and
590 dilution factors were the same as those for the fly brain immunostaining.
591
592 **Microscopy and image analysis**
593 Fly brains and mouse brain slices were scanned using a Leica TCS SP5 confocal microscope.
594 Image analysis was performed using Fiji software[77]. All analyses were conducted blindly
595 with respect to genotype.
596 *Fly brain*. TH-positive neurons were counted manually from Z-stacks of confocal
597 images using the cell counter plugin of Fiji. PAM neuron counts were scored blindly.
598 FER2::V5::GFP and TH fluorescence intensity in the PAM region was measured on Z-SUM
599 projection images. The region of interest (ROI) corresponding to the PAM cluster was
600 manually drawn to include TH^+ neurons. Background signal measured outside the ROI was
601 subtracted from the ROI signal. To quantify mitochondria circularity in PAM clusters,
602 mitoGFP-positive objects within the PAM neurons region were analyzed using a particle
603 analysis plugin as described previously[29].
604 *Mouse brain*. TH immunoreactivity in striatal regions was quantified by optical
605 densitometry using Fiji. Three striatum images were acquired for each animal, and in every
606 picture fluorescence intensity was measured for four squares drawn on the dorsal striatum
607 (n=3-4 animals per genotype). Measures from all the squares were averaged to give the value
608 for each animal. To obtain the number of mDA neurons, TH-positive neurons were counted
609 manually from Z-stacks of confocal images using the cell counter plugin (n=3 animals per
610 genotype). Every fourth section covering the entire VTA and SN in one brain hemisphere

611 was included in the counting procedure. Neuron counts were scored blindly. To quantify
612 mitochondria circularity in DA neurons, COX4-positive objects within the TH-positive DA
613 neurons were analysed using the particle analysis plugin.
614
615 **Treatment of flies with oxidative reagents**
616 7-day-old flies were placed into empty vials and starved for 6 h. The flies were then
617 transferred into vials containing *Drosophila* instant food (Formula 4-24 Instant Drosophila
618 Medium, Carolina Biological Supply Company, USA) containing 5% H_2O_2 (Sigma, H1009),
619 or vials containing *Drosophila* instant food only as a control, and kept for 24 h. All vials were
620 kept in a humid box at 25 °C during the treatment. Following the treatment, flies were
621 transferred back to the vials with standard cornmeal-agar food and maintained normally.
622 Seven days after the treatment the flies were decapitated, and anti-TH-staining was
623 performed as described above.
624
625 **ROS detection**
626 The level of ROS production in the fly brain was measured using a cell-permeable probe,
627 2'7'-dichlorofluorescin diacetate (H2DCF), following the protocol described in[78]. The
628 fluorescence intensity for the entire central brain was measured using Fiji software[77] after
629 generating a Z-SUM projection across the corresponding Z-stacks, as previously described[28].
630
631 **TMRM staining**
632 14-day-old flies expressing *UAS-GFP* driven with *R58E02-GAL4* were dissected in PBS. Fly
633 brains were incubated with 100 nM Tetramethylrhodamine methyl ester (TMRM)
634 (Invitrogen, I34361) for 30 min at 37 °C and washed three times with Hank's balanced salt
635 solution (HBSS). Brains were mounted on slides with warm HBSS. TMRM was excited with

636 561 nm and the fluorescence emission above 580 nm was measured. To quantify TMRM
637 signal within PAM neurons, PAM neurons were defined by thresholding the GFP signal
638 using Fiji software[77]. TMRM fluorescence intensity was measured within the defined volume
639 in a SUM projection of respective z-stacks.
640

641 **Startle-induced climbing assay**

642 For each experimental group, 20 male flies were briefly anesthetized with CO_2 and placed
643 into a 100 ml graduated glass cylinder, which was divided into five equal parts marked 1-5
644 from bottom to top. Flies were left to recover from the CO_2 exposure for 1 h before the assay.
645 The climbing assay was performed at ZT2 (2 h after lights-on in 12 h:12 h light-dark cycles)
646 to avoid circadian variations in the locomotor activities of the flies, following the procedure
647 previously described[28]. Briefly, the cylinder was tapped on a flexible pad to collect all of the
648 flies at the bottom, and then the flies were allowed to climb up the wall of the cylinder for 20
649 s. The number of flies that climbed up to each zone within 20 s was counted manually and
650 used to calculate the climbing index (CI) with the following formula: $CI = (0 \times n_0 + 1 \times n_1 +$
651 $2 \times n_2 + 3 \times n_3 + 4 \times n_4 + 5 \times n_5) / n_{total}$, where n_x is the number of flies that reached zone X,
652 n_0 is the number of flies that remained in the bottom of the cylinder, and n_{total} is the total
653 number of flies. Each experiment consisted of three trials, and three independent experiments
654 were performed for each genotype. The mean CI values from three independent experiments
655 are shown.
656

657 **Chromatin immunoprecipitation coupled to sequencing (ChIP-seq)**

658 ChIP was performed based on previous protocols[79,80] on *Fer2*^{1} mutant flies expressing a
659 GFP::V5-tagged *Fer2* genomic transgene (*Fer2::GFP::V5*) and on *w*^{1118} flies (negative
660 control). Briefly, ~8000 14-day-old flies per sample were collected 2 h before lights-on

661 (ZT22), frozen in liquid nitrogen and maintained at -80 °C until processed. Heads were
662 collected using metal sieves, and then, 1 ml of heads was ground in liquid nitrogen and
663 homogenized 30 times in 5 ml of NE Buffer (15 mM HEPES pH 8, 10 mM KCl, 0.1 mM
664 EDTA, 0.5 mM EGTA, 350 mM sucrose, 0.1% Tween 20, 5 mM MgCl2, 1 mM DTT, 1 mM
665 PMSF plus Protease inhibitor cocktail (Roche 11 873 580 001)) with 1% PFA. Fixation was
666 performed for 10 min at RT and quenched with 125 mM glycine for 5 min at RT. The
667 homogenate was filtered through a 100 µm nylon mesh filter (Thermo Fisher Scientific
668 22363549), and nuclei were collected by centrifugation at 800 x g for 5 min at 4 °C. The
669 nuclei were washed three times, resuspended in 1,5 ml of cold RIPA buffer (25 mM Tris-HCl
670 pH 8, 150 mM NaCl, 0,5% sodium deoxycholate, 0,1% SDS, 1% NP-40, 0,5 mM DTT plus
671 Protease inhibitor cocktail) and sonicated using a Bioruptor sonicator for 18 min (30 s ON/30
672 s OFF). The sonicated chromatin was then centrifuged at 10000 x g for 10 min at 4 °C to
673 remove cell debris. The supernatant was pre-cleared with agarose beads (1 h, 4 °C) and
674 incubated with 50 µl of saturated anti-V5 beads (Sigma A7345) overnight at 4 °C. The beads
675 were washed twice with low-salt buffer (20 mM Tris pH 8, 150 mM NaCl, 2 mM EDTA,
676 0,1% SDS, 1% Triton X-100), twice with high-salt buffer (20 mM Tris pH 8, 500 mM NaCl,
677 2 mM EDTA, 0,1% SDS, 1% Triton X-100), twice with LiCl buffer (10 mM Tris pH 8, 250
678 mM LiCl, 1 mM EDTA, 1% sodium deoxycholate, 1% NP-40) and twice with TE buffer (10
679 mM Tris-HCl pH 8, 1 mM EDTA). DNA was eluted in the V5 elution buffer (10 mM
680 HEPES, 1,5 mM MgCl2, 0,25 mM EDTA, 20% glycerol, 250 mM KCl, 0,3% NP-40, 0,5
681 mg/ml V5 peptide) and incubated with RNase (30 min, 37 °C) and proteinase K (overnight,
682 65 °C). Subsequently, the DNA was purified with a MinElute PCR purification kit (Qiagen
683 28004). Libraries were prepared with 0,5 to 0,7 ng of ChIP-enriched DNA as starting
684 material and processed using the Illumina TruSeq ChIP kit according to the manufacturer's
685 specifications, at the iGE3 Genomics Platform in Geneva. The libraries were validated on a

686 Tapestation 2200 (Agilent) and a Qubit fluorometer (Invitrogen - Thermo Fisher Scientific).
687 Single reads of 50 bp were generated using the TruSeq SBS HS v3 chemistry on an Illumina
688 HiSeq 2500 sequencer.
689
690 **ChIP-seq analysis**
691 Sequencing reads were mapped to the *Drosophila melanogaster* genome reference dm3 using
692 Bowtie2 with default settings[81]. *Fer2* binding sites were identified by individually comparing
693 each FER2 ChIP sample (N=2) to each w^{1118} ChIP sample (N=2; negative control) using
694 MACS2[82]. The minimum FDR (q-value) cutoff for peak detection was 0.05. The 267 shared
695 peaks overlapping in all the four FER2 ChIP vs w^{1118} ChIP comparisons were selected as
696 confident peaks. Peak calling was also performed using Homer[83] and over 90% of Homer
697 peaks overlapped with MACS2 peaks, confirming our results. ChIP-seq profiles were
698 visualized using IGV[84]. HOMER motif analysis algorithm was used to search for enriched
699 motifs, and identified a 12-mer containing a bHLH binding site, present in the majority of the
700 best ranked peaks. Peak-to-gene assignment was performed using the HTSstation[85] and
701 resulted in a list of 279 genes.
702
703 **Whole-head RNA-seq**
704 *hs-GAL4*, *UAS-Fer2::FLAG* flies (*hs>Fer2::FLAG*) were heat-shocked at 37 °C for 3 h, or
705 maintained at 25 °C (control), and collected 12 h or 48 h later (three independent biological
706 replicates per group). The same procedure was also applied to flies carrying *hs-GAL4* but not
707 the *UAS-Fer2,* in order to identify and exclude from our analysis the genes that responded to
708 heat irrespective of *Fer2* induction. The flies were frozen in liquid nitrogen and kept at -
709 80 °C until processed. Fly heads were collected using metal sieves and kept in Trizol (Life
710 Technologies 15596026) at -80 °C until processed. Total RNA was isolated from dissected

711 mouse brain regions using Trizol according to the manufacturer's instructions and treated
712 with Turbo DNase for 30 min at 37 °C (Turbo DNA-free kit, Thermo Fisher Scientific
713 AM1907). Libraries were prepared at the iGE3 Genomics Platform in Geneva. Single reads
714 of 50 bp were generated using an Illumina HiSeq 2500 sequencer. Data analysis was
715 performed using Galaxy[86]. Sequencing reads were mapped to the *Drosophila melanogaster*
716 genome reference dm3 using TopHat[87] with default settings. Differentially expressed genes
717 (DEG) analysis was performed with Cufflinks, Cuffmerge and Cuffdiff, to compare flies who
718 received the heat shock treatment with control flies kept at 25 °C. The same analysis was
719 performed on *hs-GAL4* flies, to identify the genes which responded to heat irrespective of
720 *Fer2* induction. These heat-responsive genes were subtracted from DEG identified in the
721 *hs>Fer2::FLAG* experiment.
722
723 **PAM-specific RNA-seq**
724 Flies carrying *R58-GAL4* were combined with *UAS-Fer2::FLAG* to overexpress *Fer2*, and
725 with *UAS-RedStinger* to mark PAM neurons. Flies carrying only *R58-GAL4* and *UAS-*
726 *RedStinger* were used as a control. Cells were dissociated from the brains of ~70 14-day-old
727 flies 2 h before lights-on (ZT22) as previously described[75], except that the brains were treated
728 with papain for 25 min. After trituration in 300 µl SMactive medium containing 50 µm AP5,
729 20 µm DNQX and 0.1 µm TTX, the cell suspension was filtered through a sterile 70 µm
730 membrane and distributed to three wells of three two-well chamber glass slides (LabTek II,
731 Nunc) kept on ice. The second well of each slide contained ice to cool the cells while
732 RedStinger-positive cells were sorted on a fluorescence microscope equipped with a
733 motorized stage and a needle holder (CellSorter Company for Innovations). Cells were
734 selected manually using capillaries with 50 µm tip diameter. Collected cells were released in
735 a clean part of the chamber and immediately picked up again, greatly reducing the amount of

736 debris, before being transferred to a fresh slide with 100 µl medium spread in a 1 × 1 cm
737 GeneFrame (Thermo Fisher Scientific). Cells were reselected for two rounds and finally
738 transferred using a new capillary with 30-µm tip diameter to 100-µl lysis buffer (Absolutely
739 RNA Nanoprep Kit; Agilent). Cells of multiple collections were pooled if needed to obtain
740 200 cells per sample, and total RNA was extracted according to the manufacturer's
741 instructions. The RNA was converted to cDNA and amplified using the SMART-Seq4 Kit
742 (Takara Bio). Libraries were generated using NexteraXT (Illumina) and sequenced on an
743 Illumina HiSeq 2500 or 4000. DEG analysis was performed using the HTSstation[85] and
744 resulted in a list of 132 genes.
745
746 **Bioinformatic analysis of genes found in ChIP-seq and RNA-seq**
747 Since human databases are generally more comprehensive, fly genes were converted into
748 human orthologs prior to Gene Ontology (GO) analysis[88]. Human orthologs of fly genes were
749 predicted using DIOPT[89] and were analyzed for GO with Metascape[88]. A network
750 representation of GO terms was obtained using Cytoscape[90]. A search for TF binding sites
751 enriched among promoters of PAM-specific RNAseq DEG was performed using PSCAN[91].
752 Protein-protein interactions were investigated using STRING[92] and a previously reported
753 *Drosophila* TFs database [49].
754
755 **Mice strains**
756 *Nato3-LoxP* mice was generated using Clustered Regularly Interspaced Short Palindromic
757 Repeats (CRISPR) technology by Applied StemCell, Inc. (Milpitas, CA). Two copies of a
758 synthetic *LoxP* sequence were inserted upstream and downstream of the unique exon of
759 *Nato3* gene. Briefly, a mixture of active guide RNA molecules (gRNAs), two single stranded
760 oligo donor nucleotides (ssODNs) and *Cas-9* mRNA was prepared and injected into the

761 cytoplasm of C57BL/6 embryos. Mice born from the microinjection were screened to identify
762 *LoxP* insertions at the designated locations using PCR and sequencing. The founder mice
763 were bred to evaluate the germline transmission and expand the *Nato3-LoxP* colonies. *DAT-*
764 *Cre* mice have been described previously[54] (obtained from Jean-Claude Martinou's
765 laboratory, University of Geneva). *DAT-Cre* and *Nato3-LoxP* mice were maintained in a
766 C57BL/6J genetic background. Crosses between these lines generated mice that are
767 homozygous for the *Nato3-LoxP* allele and harbor one copy of the *DAT-Cre* transgene
768 ($Nato3^{DAT\text{-}Cre}$). Littermates homozygous for *Nato3* floxed alleles and harboring no copy of the
769 *DAT-Cre* transgene were used as controls ($Nato3^{floxed}$). Mice were maintained in rooms with
770 controlled 12 h light/dark cycles, temperature and humidity, with food and water provided *ad*
771 *libitum*. Mice were housed at a maximum of five animals per cage in individually ventilated
772 cages. All experiments were conducted in accordance with the Institutional Animal Care and
773 Use Committee of the University of Geneva and with permission of the cantonal authorities
774 (Permit No. GE/3/19 27381, GE/78/19 31317 and GE/29/33210).
775
776 **Electron microscopy image acquisition and analysis**
777 Animals were anesthetized, perfused and embedded in agarose as described in the mouse
778 brain immunohistochemistry section, except that the perfusion was performed with 3% PFA
779 complemented with 0.2% glutaraldehyde in 0.1 M phosphate buffer (PB), pH 7.4.
780 Subsequently, 60 µm-thick sections were cut and processed for pre-embedding
781 immunoperoxidase staining, as previously described [93]. Briefly, immunostaining for DA
782 neurons in the SN was performed by incubating the sections with rabbit anti-TH antibodies
783 (Millipore ab152, 1:100) followed by goat anti-rabbit biotinylated secondary antibodies
784 (Vector Laboratories PK-4001, 1:200) and then avidin biotin peroxidase complex (Vector
785 Laboratories PK-4001). 3,3'-diaminobenzidine tetrachloride (DAB; Invitrogen Life

786 Technologies 750118) was applied for 1-2 minutes until the stain developed. Sections were
787 further embedded in EPON resin (Fluka) and trimmed around the labeled cells of interest.
788 Ultrathin (60 nm) sections were produced and imaged by a Tecnai G212 electron microscope
789 (FEI Company, Oregon, United states) equipped with a digital camera (Mega View III; Soft
790 Imaging Systems). ~15 labeled cells from two mice were analyzed for each genotype.
791 Mitochondria were classified blindly. Mitochondrial size and roundness were measured via
792 Fiji software using the particle analysis plugin after a manual selection of each
793 mitochondrion.
794
795 **RT-qPCR on mouse brain regions**
796 Animals were sacrificed by cervical dislocation and decapitated. The brains were
797 immediately removed and all the subsequent steps were performed on ice. The olfactory
798 bulbs, prefrontal cortex, striatum, cortex, and cerebellum were scalpel-dissected. The ventral
799 and dorsal midbrain were scalpel-dissected from 1 mm-thick brain slices cut in an ice-cold
800 coronal matrix (Zivic Instruments). Samples were kept in Trizol (Life Technologies
801 15596026) at -80 °C until processed. Total RNA was isolated from dissected mouse brain
802 regions using Trizol according to the manufacturer's instructions and treated with Turbo
803 DNase for 30 min at 37 °C (Turbo DNA-free kit, Thermo Fisher Scientific AM1907).
804 Reverse transcription was performed from 500 to 1000 ng RNA using the Maxima reverse
805 transcriptase (Thermo Fisher Scientific 18090050) and oligo-dT primers, according to the
806 manufacturer's instructions. Primers were designed with Primer-BLAST online tool
807 (https://www.ncbi.nlm.nih.gov/tools/primer-blast/): *B2m* (F: 5'-
808 AGAATGGGAAGCCGAACATA, R: 5'-CGTTCTTCAGCATTTGGATT), *Cyclophilin*
809 (F: 5'-TGCCATCCAGCCAGGAGGTC, R: 5'-CCATCGTGTCATCAAGGACTT), *Hmbs*
810 (F: 5'-GCTGAAAGGGCTTTTCTGAG, R: 5'-TGCCCATCTTTCATCACTGT), *Hprt1* (F:

811 5’-TGTCAGTTGCTGCGTCCCCAGA, R: 5’-TCTACCAGAGGGTAGGCTGGCC), *Pgk1*
812 (F: 5’-ACCTGCTGGCTGGATGGGCT, R: 5’-CTCGACCCACAGCCTCGGCA), *Rpl13a*
813 (F: 5’-CGGATGGTGGTCCCTGCTG, R: 5’-GAGTGGCTGTCACTGCCTGG), *Nato3* (F:
814 5’-GGTGAGCCCAAGAGACACTC, R: 5’-GTGCCGGATCCCCAACTTAT), *Engrailed 1*
815 (F: 5’-ACGCACCAGGAAGCTAAAGA, R: 5’- CTGGAACTCCGCCTTGAGTC), *Foxa1*
816 (F: 5’-GAGAGCCATCATGGTCATGTCA, R: 5’-TGGGGGTGGGGGAATCCTTTA),
817 *Foxa2* (F: 5’-CCTCAAGGCCTACGAACAGG, R: 5’-GCTTTGTTCGTGACTGGGC),
818 *Lmx1a* (F: 5’-TATACAACGTTGCCCACCCC, R: 5’- GTGATCTCCAGGCATCTGGG),
819 *Lmx1b* (F: 5’-GCAGTGGAGATGACGGGAAA, R: 5’-GAAAGCTCTTCGCTGCTGTG),
820 *Nurr1* (F: 5’-TTCCAGGCAAACCCTGACTAT, R: 5’-TGCCCACCCTCTGATGATCT).
821 Quantitative PCR (qPCR) was performed on the Light Cycler LC480 (Roche) using the TB
822 Green Ex Taq II polymerase (Takara RR820L). Each reaction was performed in triplicate.
823 Relative quantification and normalization were performed with a multiple reference genes
824 model[94]. For normalization, the best reference genes for each experiment were determined
825 using the geNorm algorithm (https://genorm.cmgg.be) within a panel of 4-5 putative
826 reference genes. To compare *Nato3* levels between different brain regions, *B2m* and
827 *cyclophilin* were used as reference genes. To compare *Nato3* levels in the midbrain between
828 different ages, *B2m* and *Hprt1* were used.
829
830 **Behavioral tests**
831 Male mice of different ages (7, 10, 13 and 16 months) were evaluated for posture control and
832 coordination (pole test), spontaneous locomotor activity (wheel test) and exploration-driven
833 locomotor behavior (open field test). All behavioral tests were performed during the light
834 cycle by experimenters blind to the genotype. The mice were allowed to habituate to the
835 behavioral room for at least 45 min before each test. Behavioral equipment was cleaned with

836 70% ethanol after each test session to avoid olfactory cues.

837 *Pole test.* The pole test was performed as previously described[56] with minor
838 modifications. Mice were first trained 4-6 times by placing the animal head-down on top of a
839 vertical pole (diameter: 1 cm, height: 55 cm) and letting it descend. Then, animals were
840 trained 3-4 times in the regular turning and descending procedure, by placing the animal
841 head-up on top of the pole. For the actual test, mice performed eight trials and were recorded
842 with a video camera. The time to orient downward (T-turn) and the total time to turn and
843 descend the pole (T-tot) were measured, with a maximum duration of 30 sec. When the
844 mouse was not able to turn downward and instead dropped from the pole in a lateral body
845 position, a value of 30 sec was assigned. The average of the eight trials was used as the final
846 score. During the training and for the real test, mice were tested a maximum of three times
847 per day, with an interval of at least 5 min between trials.

848 *Running wheel test*. Mice were singly housed in cages with free access to a running
849 wheel (14 cm in diameter) for 6 days, under a 12 h light/dark cycles. After three days of
850 habituation, the number of wheel revolutions per minute was recorded with a sensor by
851 LabVIEW program for the following three days. The total amount of time spent on the wheel
852 and the total distance run were calculated for each animal.

853 *Open field test.* Open field test was performed as previously described[13] with minor
854 modifications. The test was performed in a 40 x 40 x 40 cm arena made of white Plexiglas
855 plastic, which was illuminated from above (light intensity of 100 lux on the floor). Mice were
856 placed individually in the center of the area and allowed to freely explore it for 10 min while
857 being recorded. The horizontal locomotor activity was analyzed using the Mouse Behavioral
858 Analysis Toolbox (MouBeAT)[95] for ImageJ. The vertical activity (rearing), defined as a
859 mouse rising on its hind legs, was scored manually.

860

861 ***In situ* hybridization**

862 Mice brains were embedded in 3% low melting agarose (Topvision, R0801) and 50 μm
863 vibratome sections were mounted on Superfrost Plus slides (Thermo Scientific,
864 J1800AMNZ). The sections were fixed for 15 minutes in 10% formaldehyde, washed in PBS
865 and treated with 10 μg/ml proteinase K in TE (10 mM Tris-HCl, 1 mM EDTA, pH 8.0) for 5
866 min. The sections were fixed again in 10% formaldehyde for 10 minutes and washed in PBS,
867 then 0.2 M HCl was added to the slides for 10 min, followed by a PBS wash. The sections
868 were then pre-incubated in 0.1 M triethanolamine HCl at pH 8.0 for 1 min, incubated in 0.1
869 M triethanolamine HCl with acetic anhydride for 10 min, and then washed in PBS. Probes
870 were denatured for 7 min at 70 °C and diluted at 100nM in the hybridization buffer: 10 mM
871 NaCl, 5 mM $NaH_2PO_4 \cdot H_2O$, 5 mM $Na_2HPO_4 \cdot 2H_2O$, 5 mM EDTA, 50% formamide, 10%
872 dextran sulfate, 1 μg/μl tRNA, 1 × Denhardt's solution (Eppendorf, 0032007.155).
873 Hybridization was performed with a double DIG-labeled locked nucleic acid (LNA) probe
874 for *Nato3* (/5DiGN/ACTCAGCGTCTATCTCACCGA/3DiG_N/) (Qiagen) and incubated
875 overnight at 62 °C. The sections were washed twice for 30 minutes at 62 °C and once at room
876 temperature with 1x SSC (150mM NaCl, 15mM Sodium Citrate, pH 7.0) supplemented with
877 50% formamide and 0.1% Tween20. Slides were preincubated in 2% blocking reagent
878 (Roche, 11096176001) in MABT (100mM Maleic Acid, 150 mM NaCl, 0.1% Tween 20) for
879 20 min followed by 1 h incubation with alkaline phosphatase-anti-digoxigenin antibody
880 (1:500, Roche, 1093274). Alkaline phosphatase activity was detected by incubating slides
881 with Fast Red substrate (DAKO, K0597) for 30 minutes.

882

883 **Microdialysis and quantification of dopamine**

884 The extracellular dopamine levels in the striatum were measured using microdialysis
885 following the established method[96]. Briefly, 16- to 18-month-old mice were anaesthetized

886 with isoflurane using a controlled vaporizer. The animal was placed in a stereotaxic frame
887 and the guide cannula for the microdialysis probe was implanted in the striatum. During the
888 intervention, the animal was covered with a heating pad to keep its body temperature at
889 37 °C. An analgesic was added to its water (Dafalgan, 2 mg/ml) until the following day. 24
890 hours after the surgery, the microdialysis probe was inserted into the guide cannula, and
891 ringer solution (125 mM NaCl, 2.5 mM KCl, 1.26 mM $CaCl_2$, 1.18 mM $MgCl_2$, 0.20 mM
892 NaH_2PO_4) was perfused through the microdialysis probe at a flow at 1.0 µl/min using a high
893 precision pump. The experiments were performed during the light period and the mice were
894 tested in their home cage. After at least a 2 h equilibration period, the dialysates were
895 collected every 30 min for 2.5 h (5 samples in total). Each mouse was analyzed once.
896 Dopamine levels in the dialysates were quantified using Dopamine Research Elisa assay kit
897 (LDN Labor Diagnostika Nord GmbH & Co. KG, BA E-5300R), according to the
898 manufacturer's instructions. The absorbance at 450 nm was measured by a microplate reader
899 (Cytation 3, BioTek, Winooski, VT, USA). The dopamine concentrations were determined
900 using a standard curve.
901
902 **Statistical analysis**
903 Statistical comparisons were performed using GraphPad Prism software (San Diego, CA).
904 The statistical significance of differences between two groups was calculated using a
905 nonparametric two-tailed Mann-Whitney test. To compare three or more groups, ANOVA
906 followed by Turkey's multiple comparisons test was used. For the circularity analysis, to
907 compare the distribution of mitochondria particles between two or three genotypes, the
908 Kolmogorov-Smirnov test and the Kruskal-Wallis test followed by Dunn's test were applied,
909 respectively. Differences were considered significant at *$p<0.05$, **$p<0.01$, ***$p<0.001$,
910 ****$p<0.0001$. ns indicates not significant. Pairwise comparisons are shown as brackets.

Only where the differences are not significant and adding brackets reduces the legibility of the plots, brackets and "ns" are omitted. Box plots are used for depicting the group data comprised of fewer than 200 data points. Box boundaries are the 25th and 75th percentiles, the horizontal line across the box is the median, and the whiskers indicate the minimum and maximum values. The group data that consist of 3 data points are shown as scatter dot plots, with the horizontal line across the plot representing the mean. The group data that consist of 200 of more data points are shown as violin plots. The horizontal line across the violin plot is the median and the horizontal dotted lines represent the 25th and 75th percentiles.

DATA AVAILABILITY

The datasets generated during the current study are available in the Gene Expression Omnibus (GEO) repository. Accession numbers and the web links are as follows.

ChIP-seq data: GSE156892
(https://www.ncbi.nlm.nih.gov/geo/query/acc.cgi?acc=GSE156892)

whole-head RNA-seq data: GSE156890
(https://www.ncbi.nlm.nih.gov/geo/query/acc.cgi?acc=GSE156890)

PAM neuron RNA-seq data: GSE157589
(https://www.ncbi.nlm.nih.gov/geo/query/acc.cgi?acc=GSE157589)

ACKNOWLEDGMENTS

We thank Ernst Hafen, Chi-Hon Lee, Junhai Han, the Bloomington *Drosophila* Stock Center, the Vienna Drosophila Resource Center and the Kyoto Stock Center for fly stocks, J-C. Martinou for the *DAT-Cre* mouse strain. We thank the Genomics Platform of iGE3 for ChIP-seq and RNA-seq experiments, the animal facility of the University of Geneva for maintenance of mice colonies, and the Pole Facultaire de Microscopie Electronique (Centre

Médical Universitaire, Geneva) for electron microscopy. We are grateful to J-C. Martinou and our lab members for valuable discussions of this work. This research was supported by the European Research Council (ERC-StG-311194), the Swiss National Science Foundation (31003A_130387), the Georges and Antoine Claraz Foundation, the Novartis Foundation for Medical-Biomedical Research (19A025), the Société Académique de Genève, the Plan Stratégique Sciences Vie (PSVIE) of the University of Geneva, and the Canton of Geneva.

AUTHOR CONTRIBUTIONS

EN conceptualized the study. EN, FM, LS, DT and NL designed experiments. FM, DT, LS, NL, IN, MD, EV, FP and PBD performed experiments and analyzed data. FM, DT, LS, MD, and EN produced visualizations of the results and made figures. FM and EN wrote the manuscript.

COMPETING INTERESTS

The authors have declared that no competing interests exist.

951 **REFERENCES**

952 1. Klein, M. O. *et al.* Dopamine: Functions, Signaling, and Association with
953 Neurological Diseases. *Cell. Mol. Neurobiol.* **39**, 31–59 (2019).
954 2. Shulman, J. M., De Jager, P. L. & Feany, M. B. Parkinson's Disease: Genetics and
955 Pathogenesis. *Annu. Rev. Pathol. Mech. Dis.* **6**, 193–222 (2011).
956 3. Connolly, B. S. & Lang, A. E. Pharmacological Treatment of Parkinson Disease: A
957 Review. *JAMA* **311**, 1670 (2014).
958 4. Kalia, L. V. & Lang, A. E. Parkinson's disease. *The Lancet* **386**, 896–912 (2015).
959 5. Deng, H., Wang, P. & Jankovic, J. The genetics of Parkinson disease. *Ageing Res.*
960 *Rev.* **42**, 72–85 (2018).
961 6. Haelterman, N. A. *et al.* A Mitocentric View of Parkinson's Disease. *Annu. Rev.*
962 *Neurosci.* **37**, 137–159 (2014).
963 7. Von Stockum, S., Nardin, A., Schrepfer, E. & Ziviani, E. Mitochondrial dynamics
964 and mitophagy in Parkinson's disease: A fly point of view. *Neurobiol. Dis.* **90**, 58–67 (2016).
965 8. Sonnier, L. *et al.* Progressive Loss of Dopaminergic Neurons in the Ventral Midbrain
966 of Adult Mice Heterozygote for Engrailed1. *J. Neurosci.* **27**, 1063–1071 (2007).
967 9. Laguna, A. *et al.* Dopaminergic control of autophagic-lysosomal function implicates
968 Lmx1b in Parkinson's disease. *Nat. Neurosci.* **18**, 826–835 (2015).
969 10. Doucet-Beaupré, H. *et al.* Lmx1a and Lmx1b regulate mitochondrial functions and
970 survival of adult midbrain dopaminergic neurons. *Proc. Natl. Acad. Sci.* **113**, E4387–E4396
971 (2016).
972 11. Kittappa, R., Chang, W. W., Awatramani, R. B. & McKay, R. D. G. The foxa2 Gene
973 Controls the Birth and Spontaneous Degeneration of Dopamine Neurons in Old Age. *PLoS*
974 *Biol.* **5**, e325 (2007).
975 12. Domanskyi, A., Alter, H., Vogt, M. A., Gass, P. & Vinnikov, I. A. Transcription
976 factors Foxa1 and Foxa2 are required for adult dopamine neurons maintenance. *Front. Cell.*
977 *Neurosci.* **8**, (2014).
978 13. Kadkhodaei, B. *et al.* Transcription factor Nurr1 maintains fiber integrity and nuclear-
979 encoded mitochondrial gene expression in dopamine neurons. *Proc. Natl. Acad. Sci.* **110**,
980 2360–2365 (2013).
981 14. van den Munckhof, P. *et al.* Pitx3 is required for motor activity and for survival of a
982 subset of midbrain dopaminergic neurons. *Dev. Camb. Engl.* **130**, 2535–2542 (2003).
983 15. Di Salvio, M. *et al.* Otx2 controls neuron subtype identity in ventral tegmental area
984 and antagonizes vulnerability to MPTP. *Nat. Neurosci.* **13**, 1481–1488 (2010).
985 16. Blaudin de Thé, F. *et al.* Engrailed homeoprotein blocks degeneration in adult
986 dopaminergic neurons through LINE-1 repression. *EMBO J.* **37**, (2018).
987 17. Le, W. *et al.* Mutations in NR4A2 associated with familial Parkinson disease. *Nat.*
988 *Genet.* **33**, 85–89 (2003).
989 18. Bergman, O. *et al.* Do polymorphisms in transcription factors LMX1A and LMX1B
990 influence the risk for Parkinson's disease? *J. Neural Transm.* **116**, 333–338 (2009).
991 19. Oh, S. *et al.* Combined Nurr1 and Foxa2 roles in the therapy of Parkinson's disease.
992 *EMBO Mol. Med.* **7**, 510–525 (2015).
993 20. Alvarez-Fischer, D. *et al.* Engrailed protects mouse midbrain dopaminergic neurons
994 against mitochondrial complex I insults. *Nat. Neurosci.* **14**, 1260–1266 (2011).
995 21. Di Giovannantonio, L. G. *et al.* Otx2 selectively controls the neurogenesis of specific
996 neuronal subtypes of the ventral tegmental area and compensates En1-dependent neuronal
997 loss and MPTP vulnerability. *Dev. Biol.* **373**, 176–183 (2013).
998 22. Hewitt, V. L. & Whitworth, A. J. Mechanisms of Parkinson's Disease. in *Current*
999 *Topics in Developmental Biology* vol. 121 173–200 (Elsevier, 2017).
1000 23. Nagoshi, E. Drosophila Models of Sporadic Parkinson's Disease. *Int. J. Mol. Sci.* **19**,

1001 3343 (2018).
1002 24. Landayan, D. & Wolf, F. W. Shared neurocircuitry underlying feeding and drugs of
1003 abuse in Drosophila. *Biomed. J.* **38**, 496–509 (2015).
1004 25. Strausfeld, N. J. & Hirth, F. Deep Homology of Arthropod Central Complex and
1005 Vertebrate Basal Ganglia. *Science* **340**, 157–161 (2013).
1006 26. Liu, C. *et al.* A subset of dopamine neurons signals reward for odour memory in
1007 Drosophila. *Nature* **488**, 512–516 (2012).
1008 27. Riemensperger, T. *et al.* A Single Dopamine Pathway Underlies Progressive
1009 Locomotor Deficits in a Drosophila Model of Parkinson Disease. *Cell Rep.* **5**, 952–960
1010 (2013).
1011 28. Bou Dib, P. *et al.* A Conserved Role for p48 Homologs in Protecting Dopaminergic
1012 Neurons from Oxidative Stress. *PLoS Genet.* **10**, e1004718 (2014).
1013 29. Tas, D. *et al.* Parallel roles of transcription factors dFOXO and FER2 in the
1014 development and maintenance of dopaminergic neurons. *PLOS Genet.* **14**, e1007271 (2018).
1015 30. Lawal, H. O. *et al.* The Drosophila vesicular monoamine transporter reduces
1016 pesticide-induced loss of dopaminergic neurons. *Neurobiol. Dis.* **40**, 102–112 (2010).
1017 31. Sun, J. *et al.* Neural Control of Startle-Induced Locomotion by the Mushroom Bodies
1018 and Associated Neurons in Drosophila. *Front. Syst. Neurosci.* **12**, 6 (2018).
1019 32. Y. Ono, Nakatani, T., Minaki, Y. & Kumai, M. The basic helix-loop-helix
1020 transcription factor Nato3 controls neurogenic activity in mesencephalic floor plate cells.
1021 *Development* **137**, 1897–1906 (2010).
1022 33. Nissim-Eliraz, E., Zisman, S., Schatz, O. & Ben-Arie, N. Nato3 Integrates with the
1023 Shh-Foxa2 Transcriptional Network Regulating the Differentiation of Midbrain
1024 Dopaminergic Neurons. *J. Mol. Neurosci.* **51**, 13–27 (2013).
1025 34. Mansour, A. A., Khazanov-Zisman, S., Netser, Y., Klar, A. & Ben-Arie, N. Nato3
1026 plays an integral role in dorsoventral patterning of the spinal cord by segregating floor
1027 plate/p3 fates via Nkx2.2 suppression and Foxa2 maintenance. *Development* **141**, 574–584
1028 (2014).
1029 35. Zimprich, A. *et al.* Mutations in LRRK2 Cause Autosomal-Dominant Parkinsonism
1030 with Pleomorphic Pathology. *Neuron* **44**, 601–607 (2004).
1031 36. Langston, R. G., Rudenko, I. N. & Cookson, M. R. The function of orthologues of the
1032 human Parkinson's disease gene LRRK2 across species: implications for disease modelling
1033 in preclinical research. *Biochem. J.* **473**, 221–232 (2016).
1034 37. Kitada, T. *et al.* Mutations in the parkin gene cause autosomal recessive juvenile
1035 parkinsonism. *Nature* **392**, 605–608 (1998).
1036 38. Cha, G.-H. *et al.* Parkin negatively regulates JNK pathway in the dopaminergic
1037 neurons of Drosophila. *Proc. Natl. Acad. Sci.* **102**, 10345–10350 (2005).
1038 39. Park, J. *et al.* Mitochondrial dysfunction in Drosophila PINK1 mutants is
1039 complemented by parkin. *Nature* **441**, 1157–1161 (2006).
1040 40. Park, J., Lee, G. & Chung, J. The PINK1–Parkin pathway is involved in the
1041 regulation of mitochondrial remodeling process. *Biochem. Biophys. Res. Commun.* **378**, 518–
1042 523 (2009).
1043 41. Greene, J. C. *et al.* Mitochondrial pathology and apoptotic muscle degeneration in
1044 Drosophila parkin mutants. *Proc. Natl. Acad. Sci.* **100**, 4078–4083 (2003).
1045 42. Clark, I. E. *et al.* Drosophila pink1 is required for mitochondrial function and interacts
1046 genetically with parkin. *Nature* **441**, 1162–1166 (2006).
1047 43. Poole, A. C. *et al.* The PINK1/Parkin pathway regulates mitochondrial morphology.
1048 *Proc. Natl. Acad. Sci.* **105**, 1638–1643 (2008).
1049 44. Scialò, F. *et al.* Mitochondrial ROS Produced via Reverse Electron Transport Extend
1050 Animal Lifespan. *Cell Metab.* **23**, 725–734 (2016).

1051 45. Croset, V., Treiber, C. D. & Waddell, S. Cellular diversity in the Drosophila midbrain
1052 revealed by single-cell transcriptomics. *eLife* **7**, e34550 (2018).
1053 46. Davie, K. *et al.* A Single-Cell Transcriptome Atlas of the Aging Drosophila Brain.
1054 *Cell* **174**, 982-998.e20 (2018).
1055 47. Spivakov, M. Spurious transcription factor binding: non-functional or genetically
1056 redundant? *BioEssays News Rev. Mol. Cell. Dev. Biol.* **36**, 798–806 (2014).
1057 48. Flynn, J. M. & Melov, S. SOD2 in mitochondrial dysfunction and neurodegeneration.
1058 *Free Radic. Biol. Med.* **62**, 4–12 (2013).
1059 49. Shokri, L. *et al.* A Comprehensive Drosophila melanogaster Transcription Factor
1060 Interactome. *Cell Rep.* **27**, 955-970.e7 (2019).
1061 50. Zhu, J., Chen, L., Sun, G. & Raikhel, A. S. The Competence Factor Ftz-F1 Potentiates
1062 Ecdysone Receptor Activity via Recruiting a p160/SRC Coactivator. *Mol. Cell. Biol.* **26**,
1063 9402–9412 (2006).
1064 51. Xie, X.-J. *et al.* CDK8-Cyclin C Mediates Nutritional Regulation of Developmental
1065 Transitions through the Ecdysone Receptor in Drosophila. *PLoS Biol.* **13**, e1002207 (2015).
1066 52. Peterson, D. J. *et al.* The Basic Helix-Loop-Helix Gene Nato3 Drives Expression of
1067 Dopaminergic Neuron Transcription Factors in Neural Progenitors. *Neuroscience* **421**, 176–
1068 191 (2019).
1069 53. GTEx Consortium. The Genotype-Tissue Expression (GTEx) project. *Nat. Genet.* **45**,
1070 580–585 (2013).
1071 54. Turiault, M. *et al.* Analysis of dopamine transporter gene expression pattern --
1072 generation of DAT-iCre transgenic mice. *FEBS J.* **274**, 3568–3577 (2007).
1073 55. Engblom, D. *et al.* Glutamate receptors on dopamine neurons control the persistence
1074 of cocaine seeking. *Neuron* **59**, 497–508 (2008).
1075 56. Matsuura, K., Kabuto, H., Makino, H. & Ogawa, N. Pole test is a useful method for
1076 evaluating the mouse movement disorder caused by striatal dopamine depletion. *J. Neurosci.*
1077 *Methods* **73**, 45–48 (1997).
1078 57. Gould, T. D., Dao, D. T. & Kovacsics, C. E. The open field test. in *Mood and anxiety*
1079 *related phenotypes in mice: Characterization using behavioral tests* 1–20 (Humana Press,
1080 2009). doi:10.1007/978-1-60761-303-9_1.
1081 58. Moore, A. W., Barbel, S., Jan, L. Y. & Jan, Y. N. A genomewide survey of basic
1082 helix-loop-helix factors in Drosophila. *Proc. Natl. Acad. Sci.* **97**, 10436–10441 (2000).
1083 59. Segev, E., Halachmi, N., Salzberg, A. & Ben-Arie, N. Nato3 is an evolutionarily
1084 conserved bHLH transcription factor expressed in the CNS of Drosophila and mouse. *Mech.*
1085 *Dev.* **106**, 197–202 (2001).
1086 60. Verzi, M. P. *et al.* N-twist, an evolutionarily conserved bHLH protein expressed in
1087 the developing CNS, functions as a transcriptional inhibitor. *Dev. Biol.* **249**, 174–190 (2002).
1088 61. Khazanov, S. *et al.* Floor plate descendants in the ependyma of the adult mouse
1089 Central Nervous System. *Int. J. Dev. Biol.* **61**, 257–265 (2017).
1090 62. Arenas, E., Denham, M. & Villaescusa, J. C. How to make a midbrain dopaminergic
1091 neuron. *Development* **142**, 1918–1936 (2015).
1092 63. Toledo, E. M. *et al.* Srebf1 Controls Midbrain Dopaminergic Neurogenesis. *Cell Rep.*
1093 **31**, 107601 (2020).
1094 64. Metzakopian, E. *et al.* Genome-wide characterization of Foxa2 targets reveals
1095 upregulation of floor plate genes and repression of ventrolateral genes in midbrain
1096 dopaminergic progenitors. *Dev. Camb. Engl.* **139**, 2625–2634 (2012).
1097 65. Do, C. B. *et al.* Web-Based Genome-Wide Association Study Identifies Two Novel
1098 Loci and a Substantial Genetic Component for Parkinson's Disease. *PLOS Genet.* **7**,
1099 e1002141 (2011).
1100 66. Shulman, J. M. *et al.* Association of Parkinson disease risk loci with mild

1101 parkinsonian signs in older persons. *JAMA Neurol.* **71**, 429–435 (2014).
1102 67. Vilain, S. *et al.* The Yeast Complex I Equivalent NADH Dehydrogenase Rescues
1103 pink1 Mutants. *PLoS Genet.* **8**, e1002456 (2012).
1104 68. Pogson, J. H. *et al.* The complex I subunit NDUFA10 selectively rescues Drosophila
1105 pink1 mutants through a mechanism independent of mitophagy. *PLoS Genet.* **10**, e1004815
1106 (2014).
1107 69. Biosa, A. *et al.* Superoxide dismutating molecules rescue the toxic effects of PINK1
1108 and parkin loss. *Hum. Mol. Genet.* **27**, 1618–1629 (2018).
1109 70. Mahlknecht, P., Seppi, K. & Poewe, W. The Concept of Prodromal Parkinson's
1110 Disease. *J. Park. Dis.* **5**, 681–697 (2015).
1111 71. Bishop, M. W. *et al.* Hyperexcitable substantia nigra dopamine neurons in PINK1-
1112 and HtrA2/Omi-deficient mice. *J. Neurophysiol.* **104**, 3009–3020 (2010).
1113 72. Itier, J.-M. *et al.* Parkin gene inactivation alters behaviour and dopamine
1114 neurotransmission in the mouse. *Hum. Mol. Genet.* **12**, 2277–2291 (2003).
1115 73. Carvey, P. M., Punati, A. & Newman, M. B. Progressive dopamine neuron loss in
1116 Parkinson's disease: the multiple hit hypothesis. *Cell Transplant.* **15**, 239–250 (2006).
1117 74. Spathis, A. D. *et al.* Nurr1:RXRα heterodimer activation as monotherapy for
1118 Parkinson's disease. *Proc. Natl. Acad. Sci. U. S. A.* **114**, 3999–4004 (2017).
1119 75. Nagoshi, E. *et al.* Dissecting differential gene expression within the circadian
1120 neuronal circuit of Drosophila. *Nat. Neurosci.* **13**, (2010).
1121 76. Imai, Y. *et al.* Phosphorylation of 4E-BP by LRRK2 affects the maintenance of
1122 dopaminergic neurons in Drosophila. *EMBO J.* **27**, 2432–2443 (2008).
1123 77. Schindelin, J. *et al.* Fiji - an Open Source platform for biological image analysis. *Nat.*
1124 *Methods* **9**, (2012).
1125 78. Owusu-Ansah, E., Yavari, A. & Banerjee, U. A protocol for in vivo detection of
1126 reactive oxygen species. *Protoc. Exch.* (2008) doi:10.1038/nprot.2008.23.
1127 79. Meireles-Filho, A. C. A., Bardet, A. F., Yáñez-Cuna, J. O., Stampfel, G. & Stark, A.
1128 cis-regulatory requirements for tissue-specific programs of the circadian clock. *Curr. Biol.*
1129 *CB* **24**, 1–10 (2014).
1130 80. Zhou, J., Yu, W. & Hardin, P. E. ChIPping away at the Drosophila clock. *Methods*
1131 *Enzymol.* **551**, 323–347 (2015).
1132 81. Langmead, B. & Salzberg, S. L. Fast gapped-read alignment with Bowtie 2. *Nat.*
1133 *Methods* **9**, 357–359 (2012).
1134 82. Feng, J., Liu, T., Qin, B., Zhang, Y. & Liu, X. S. Identifying ChIP-seq enrichment
1135 using MACS. *Nat. Protoc.* **7**, (2012).
1136 83. Heinz, S. *et al.* Simple combinations of lineage-determining transcription factors
1137 prime cis-regulatory elements required for macrophage and B cell identities. *Mol. Cell* **38**,
1138 576–589 (2010).
1139 84. Robinson, J. T. *et al.* Integrative genomics viewer. *Nat. Biotechnol.* **29**, 24–26 (2011).
1140 85. David, F. P. A. *et al.* HTSstation: A Web Application and Open-Access Libraries for
1141 High-Throughput Sequencing Data Analysis. *PLOS ONE* **9**, e85879 (2014).
1142 86. Afgan, E. *et al.* The Galaxy platform for accessible, reproducible and collaborative
1143 biomedical analyses: 2018 update. *Nucleic Acids Res.* **46**, W537–W544 (2018).
1144 87. Kim, D. *et al.* TopHat2: accurate alignment of transcriptomes in the presence of
1145 insertions, deletions and gene fusions. *Genome Biol.* **14**, R36 (2013).
1146 88. Zhou, Y. *et al.* Metascape provides a biologist-oriented resource for the analysis of
1147 systems-level datasets. *Nat. Commun.* **10**, 1523 (2019).
1148 89. Hu, Y. *et al.* An integrative approach to ortholog prediction for disease-focused and
1149 other functional studies. *BMC Bioinformatics* **12**, 357 (2011).
1150 90. Shannon, P. *et al.* Cytoscape: a software environment for integrated models of

1151 biomolecular interaction networks. *Genome Res.* **13**, 2498–2504 (2003).
1152 91. Zambelli, F., Pesole, G. & Pavesi, G. Pscan: finding over-represented transcription
1153 factor binding site motifs in sequences from co-regulated or co-expressed genes. *Nucleic*
1154 *Acids Res.* **37**, W247-252 (2009).
1155 92. Szklarczyk, D. *et al.* STRING v11: protein-protein association networks with
1156 increased coverage, supporting functional discovery in genome-wide experimental datasets.
1157 *Nucleic Acids Res.* **47**, D607–D613 (2019).
1158 93. Nikonenko, I. *et al.* PSD-95 promotes synaptogenesis and multiinnervated spine
1159 formation through nitric oxide signaling. *J. Cell Biol.* **183**, 1115–1127 (2008).
1160 94. Hellemans, J., Mortier, G., De Paepe, A., Speleman, F. & Vandesompele, J. qBase
1161 relative quantification framework and software for management and automated analysis of
1162 real-time quantitative PCR data. *Genome Biol.* **8**, R19 (2007).
1163 95. Bello-Arroyo, E. *et al.* MouBeAT: A New and Open Toolbox for Guided Analysis of
1164 Behavioral Tests in Mice. *Front. Behav. Neurosci.* **12**, 201 (2018).
1165 96. Petrelli, F. *et al.* Dysfunction of homeostatic control of dopamine by astrocytes in the
1166 developing prefrontal cortex leads to cognitive impairments. *Mol. Psychiatry* **25**, 732–749
1167 (2020).
1168
1169

1170 **FIGURE LEGENDS**

1171 **Figure 1. *Fer2* overexpression prevents the loss of PAM dopaminergic neurons and**
1172 **mitochondrial dysfunction in genetic models of PD.**

1173 **(a and b)** *Fer2* overexpression prevented the loss of PAM neurons induced by the targeted
1174 expression of wild-type (*WT*) or pathogenic mutant *Lrrk* in PAM neurons. **(a)** Representative
1175 images of PAM neurons at day 14 detected by anti-TH antibodies (green). *PAM*, PAM
1176 neuron-specific *R58E02-GAL4* driver. *PAM>X* indicates that *UAS-transgene X* is driven by
1177 *R58E02-GAL4*. Scale bar, 20 μm. Top left, a schematic of DA neurons in the PAM (green)
1178 and other clusters (black). **(b)** Quantification of the number of TH^+ PAM neurons per
1179 hemisphere from (**a**). The elements of the box plots are as defined in the Method section.
1180 n=14-20 hemispheres per group. **p<0.01, ***p<0.001, ****p<0.0001. ns, not significant.
1181 One-way ANOVA followed by a Turkey's test for multiple group comparison. **(c)**
1182 Representative images of PAM neurons at day 14 labeled by *PAM>Red Stinger* expression
1183 (green). Scale bar, 20 μm. **(d)** Quantification of the number of Red $Stinger^+$ PAM neurons per
1184 hemisphere from (**c**). n=14-20 hemispheres per group. ****p<0.0001. ns, not significant.
1185 One-way ANOVA followed by a Turkey's test for multiple group comparison. **(e)** The
1186 mitochondrial network in PAM neurons was visualized using mitoGFP. Scale bar, 5 μm. **(f)**
1187 Top, histograms showing the circularity distribution of GFP^+ particles measured from (**e**).
1188 Bottom, the Gaussian curve fit to the circularity histogram. Circularity ranges from 0
1189 (reticular mitochondria) to 1 (round mitochondria). The histogram of *PAM>mitoGFP, park*^{1}
1190 is right-shifted compared with those of *PAM>mitoGFP, park*^{1}/+ and *PAM>mitoGFP, Fer2,*
1191 *park*^{1}, indicating the accumulation of rounder mitochondria in *park*^{1} and its rescue by *Fer2*.
1192 ****p<0.0001 using Kruskal-Wallis test followed by Dunn's test for multiple group
1193 comparison. More than 500 mitochondrial particles were analyzed from 14-20 hemispheres
1194 per genotype. **(g)** Quantification of TMRM fluorescence intensity in GFP-labeled PAM

1195 neurons in 14-days-old flies. n=14-20 hemispheres per group. **p<0.01. ns, not significant.
1196 One-way ANOVA followed by a Turkey's test for multiple group comparison.
1197
1198 **Figure 2. *Fer2* overexpression protects PAM dopaminergic neurons from oxidative**
1199 **insults.**
1200 **(a)** w^{1118}, $Fer2^2/+$, $Fer2^2$, *R58E02-GAL4* (*PAM*) and PAM>*Fer2* flies were fed with H_2O_2 at
1201 day 7 for 24 h and the number of PAM neurons was examined at day 14. *Fer2* mutation
1202 exacerbates, whereas *Fer2* overexpression prevents, H_2O_2-induced PAM neuron loss. n=14-
1203 20 hemispheres per group. Mann-Whitney test, **p<0.01, ***p<0.001, ****p<0.0001. **(b)**
1204 ROS levels in w^{1118} flies at different ages were monitored using H2DCF dye. Scale bar, 25
1205 μm. **(c)** Quantification of ROS levels in the central brain from (**b**). Data are represented as
1206 fold change relative to day 1. n=14-20 hemispheres per group. One-way ANOVA followed
1207 by a Turkey's test for multiple group comparison, **p<0.01. **(d)** Brains of *Fer2::GFP::V5*
1208 flies of different ages were stained with anti-GFP (green) and PAM neurons were detected by
1209 anti-TH antibodies (magenta). Scale bar, 5 μm. **(e)** GFP and TH fluorescence intensities in
1210 the PAM region from (**d**) were quantified. Data are represented as fold change relative to day
1211 1. n=14-20 hemispheres per group. One-way ANOVA followed by a Turkey's test for
1212 multiple group comparison, *p<0.05, ****p<0.0001.
1213
1214 **Figure 3. Identification of *Fer2* transcriptional targets through a combination of ChIP-**
1215 **seq and RNA-seq approaches.**
1216 **(a)** ChIP-seq was performed on 14-day-old *Fer2::GFP::V5*, $Fer2^1$ flies. w^{1118} flies were used
1217 as a negative control. Two biological replicates per group. **(b)** A sequence containing an E-
1218 box (CANNTG, underlined) was found enriched in FER2 ChIP-seq peaks over w^{1118} ChIP-
1219 seq. **(c)** Scheme of the whole-head RNA-seq analysis to identify DEG after heat shock-driven

1220 *Fer2* transient overexpression. Three biological replicates per group. The number of DEGs
1221 up- and downregulated after heat shock are shown**. (d)** Examples of ChIP-seq and RNA-seq
1222 data (48 h) for two *Fer2* direct targets, *CG8128* and *skd*. The rectangles indicate ChIP-seq
1223 peaks.
1224
1225 **Figure 4. *Fer2* targets contribute to PAM neurons maintenance and mitochondrial**
1226 **health.**
1227 **(a)** Scheme of RNA-seq analysis of isolated PAM neurons to identify genes regulated by
1228 *Fer2* constitutive overexpression. Three biological replicates per group. **(b)** Intersection
1229 between peak-associated genes identified by FER2 ChIP-seq, DEG identified by whole-head
1230 RNA-seq 48 h after heat shock, and genes expressed in PAM neuron RNA-seq. **(c)** Network
1231 visualization of the 26 *Fer2* direct targets expressed in PAM neurons and their interactions.
1232 Each node represents a gene and is colored based on its function. The shape of the node
1233 indicates whether the gene is up- or downregulated by *Fer2.* The line thickness indicates the
1234 strength of data support. **(d)** Position of FER2 peaks and effect of *Fer2* overexpression on the
1235 expression of *Fer2* direct targets. **(e)** Volcano plot of 48 h heat shock RNA-seq data. Orange
1236 (downregulated) and blue (upregulated) dots indicate the 26 *Fer2* direct targets. **(f)**
1237 Functional validation of *Fer2* direct targets regarding their effect on PAM neuron survival.
1238 Quantification of the number of PAM neurons per hemisphere detected by anti-TH
1239 immunostaining in 35-day-old flies, upon overexpression (OE) or knock-down (RNAi) of the
1240 indicated gene in PAM neurons. n=14-20 hemispheres per group. Genes that cause a
1241 statistically significant loss of PAM neurons are highlighted in red. A second independent
1242 replicate was assessed for these genes to confirm the significant loss of PAM neurons. One-
1243 way ANOVA followed by a Dunnett's test for multiple group comparison, **$p<0.01$,
1244 ****$p<0.0001$. **(g)** Network visualization of the most enriched GO terms among up-regulated

1245 and down-regulated DEGs in PAM RNA-seq. GO terms were grouped into clusters based on
1246 their membership similarities. Each node represents a GO term and is colored based on its
1247 cluster ID. GO terms that did not cluster are not shown. **(h)** Quantification of the number of
1248 PAM neurons per hemisphere, as detected by anti-TH immunostaining for the indicated
1249 genotypes and ages. *Sod2* overexpression in PAM neurons partially rescues PAM neuron loss
1250 in *Fer2*^{2} mutants. n=14-20 hemispheres per group. One-way ANOVA followed by a
1251 Turkey's test for multiple group comparison, *p<0.05, ****p<0.0001.
1252
1253 **Figure 5. *Nato3* is expressed in the midbrain DA neurons in adult mice. (a)** Phylogenetic
1254 tree generated by multiple protein sequence alignment of *Drosophila* FER2 and mouse
1255 TCF15, NATO3, PTF1A and TWIST1, using ClustalW. **(b)** *NATO3* expression levels in
1256 human tissues measured by RNA-seq as reported in GTEx portal (gtexportal.org). **(c)** RT-
1257 qPCR analysis of *Nato3* mRNA expression levels in different brain regions of C57BL6 mice
1258 at 4 months. OB, olfactory bulbs. PFC, prefrontal cortex. vMB, ventral midbrain. dMB,
1259 dorsal midbrain. Data are represented as scatter dot plots, with the horizontal line
1260 representing the mean. n=3 animals per region. One-way ANOVA followed by a Turkey's
1261 test for multiple group comparison, vMB vs any region other than dMB ***p<0.001, dMB vs
1262 any other region than vMB and cerebellum **p<0.01, dMB vs cerebellum #p<0.05. **(d)** RT-
1263 qPCR analysis of *Nato3* mRNA expression levels in the ventral midbrain of C57BL6 mice at
1264 different ages. Data are represented as scatter dot plots, with the horizontal line representing
1265 the mean of the fold change relative to the expression at 1 month. n=3-5 animals per group.
1266 No statistically significant difference between different ages by ANOVA. **(e)** Representative
1267 images of *Nato3* (magenta) *in situ* hybridization in coronal sections of the ventral midbrain of
1268 4-month-old C57BL6 mice. mDA neurons were detected by anti-TH antibodies (green).
1269 Scale bar, 10 μm.

1270

1271 **Figure 6. *Nato3* cKO in DA neurons leads to age-dependent impairment in locomotor**

1272 **coordination and activity.**

1273 **(a)** Strategy for conditional ablation of *Nato3* in differentiated DA neurons. **(b)** RT-qPCR

1274 analysis of *Nato3* mRNA levels in ventral midbrains of 2-month-old *Nato3*^{floxed} (ctrl) and

1275 *Nato3*$^{DAT\text{-}Cre}$ (cKO) mice. Data are represented as fold change relative to the expression in the

1276 ctrl. n=5-6 mice per genotype. Mann-Whitney test, *p<0.05. **(c)** Representative images of

1277 *Nato3* (magenta) *in situ* hybridization in coronal sections of the ventral midbrain of 4-month-

1278 old control and *Nato3* cKO mice. mDA neurons were detected by anti-TH antibodies (green).

1279 Scale bar, 10 µm. **(d)** The percentage of TH^{+} mDA neurons that express *Nato3* was

1280 quantified from *in situ* hybridization experiments. More than 300 TH^{+} neurons per genotype

1281 were analyzed. **(e)** The motor coordination of control and *Nato3* cKO mice was assessed at

1282 different ages using the pole test. The time taken to orient downward at the top of the pole (T-

1283 turn; left) and the total time to turn and descend the pole (T-tot; right) are shown. n=7-11

1284 mice per group. Mann-Whitney test comparing ctrl and cKO of the same age, *p<0.05,

1285 **p<0.01. ns, not significant. **(f)** Locomotor activity assessed at different ages using the

1286 voluntary wheel running test. The time spent running on the wheel (left) and the total

1287 distance run (right) are shown. n=7-11 mice per group. Mann-Whitney test comparing ctrl

1288 and cKO of the same age, *p<0.05. ns, not significant. **(g)** Representative TH

1289 immunostaining images of coronal ventral midbrain sections from 16- to 18-month-old

1290 control and *Nato3* cKO mice. Scale bar, 200µm. **(h)** Quantification of TH^{+} neurons in SN and

1291 VTA from (**g**). Data are represented as scatter dot plots, with the horizontal line representing

1292 the mean of the fold change relative to the expression in the ctrl. n=3 mice per genotype. No

1293 statistically significant difference between ctrl and cKO by Mann-Whitney test. **(i)**

1294 Representative TH immunostaining images of coronal striatal sections from 16- to 18-month-

1295 old control and *Nato3* cKO mice. Scale bar, 200µm. **(j)** Optical densitometry from TH
1296 immunostaining of the dorsal striatum in (**i**). Data are represented as fold change relative to
1297 the expression level in the ctrl. n=4 mice per genotype. No statistically significant difference
1298 between ctrl and cKO by Mann-Whitney test. **(k)** Basal levels of extracellular DA (ng/µl) in
1299 microdialysis perfusate from striatum of control and *Nato3* cKO mice. Data are represented
1300 as fold change relative to ctrl. n=4 mice per genotype. No statistically significant difference
1301 between ctrl and cKO by Mann-Whitney test.
1302
1303 **Figure 7. *Nato3* is essential for mitochondrial integrity in the midbrain DA neurons.**
1304 **(a)** Mitochondria were visualized by anti-COX4 immunostaining (magenta) in TH^+ neurons
1305 (green) of SN in 16- to 18-month-old control and *Nato3* cKO mice. Scale bar, 10 µm. **(b)** The
1306 circularity of $COX4^+$ mitochondria particles in TH^+ neurons from (**a**) was measured and its
1307 distribution was plotted in a histogram. The histogram for the *Nato3* cKO mouse is
1308 significantly right shifted compared with that of the control. Kolmogorov-Smirnov test,
1309 $p<0.0001$. More than 700 $COX4^+$ particles per genotype were analyzed from three brains per
1310 genotype. **(c)** Electron micrographs of mitochondria from TH-labeled DA neurons from the
1311 SN of 16- to 18-month-old control and *Nato3* cKO mice. The right bottom panel illustrates
1312 the difference between a degenerating mitochondrion in the dendrite of a *Nato3*-ablated TH^+
1313 neuron, and a normal mitochondrion in an adjacent non-DA neuron. M, normal mitochondria.
1314 DM, degenerative mitochondria. Scale bar, 0.5 µm. **(d)** Classification criteria for
1315 mitochondria integrity (top) and mitochondria distribution in TH^+ neurons in 6-month-old
1316 and 16- to18-month-old control and *Nato3* cKO mice (bottom). In total, 200 to 350
1317 mitochondria from TH^+ neurons in SN were analyzed per group. **(e)** Measurement of size
1318 (left) and roundness (right) of mitochondria. 200 to 350 mitochondria from SN TH^+ neurons
1319 were analyzed per group. The horizontal line across the violin plot is the median. One-way

1320 ANOVA followed by a Turkey's test for multiple group comparison, *p<0.05. ns, not
1321 significant. **(f)** Representative images of anti-SOD2 (magenta) immunostaining in coronal
1322 sections of the ventral midbrain of 16- to 18-month-old mice. mDA neurons were detected by
1323 anti-TH antibodies (green). Scale bar, 10 µm. **(g)** SOD2 fluorescence intensities in TH^+
1324 neurons from (**f**) were quantified. The horizontal line across the violin plot is the median. 300
1325 to 500 TH^+ neurons per genotype were analyzed from three brains per genotype. Mann-
1326 Whitney test, ****p<0.0001. **(h)** RT-qPCR analysis of neuroprotective transcription factors
1327 mRNA levels in ventral midbrains of 16- to 18-month-old control and *Nato3* cKO mice. Data
1328 are represented as fold change relative to the expression in ctrl. n=4 mice per genotype.
1329 Mann-Whitney test, *p<0.05. ns, not significant.

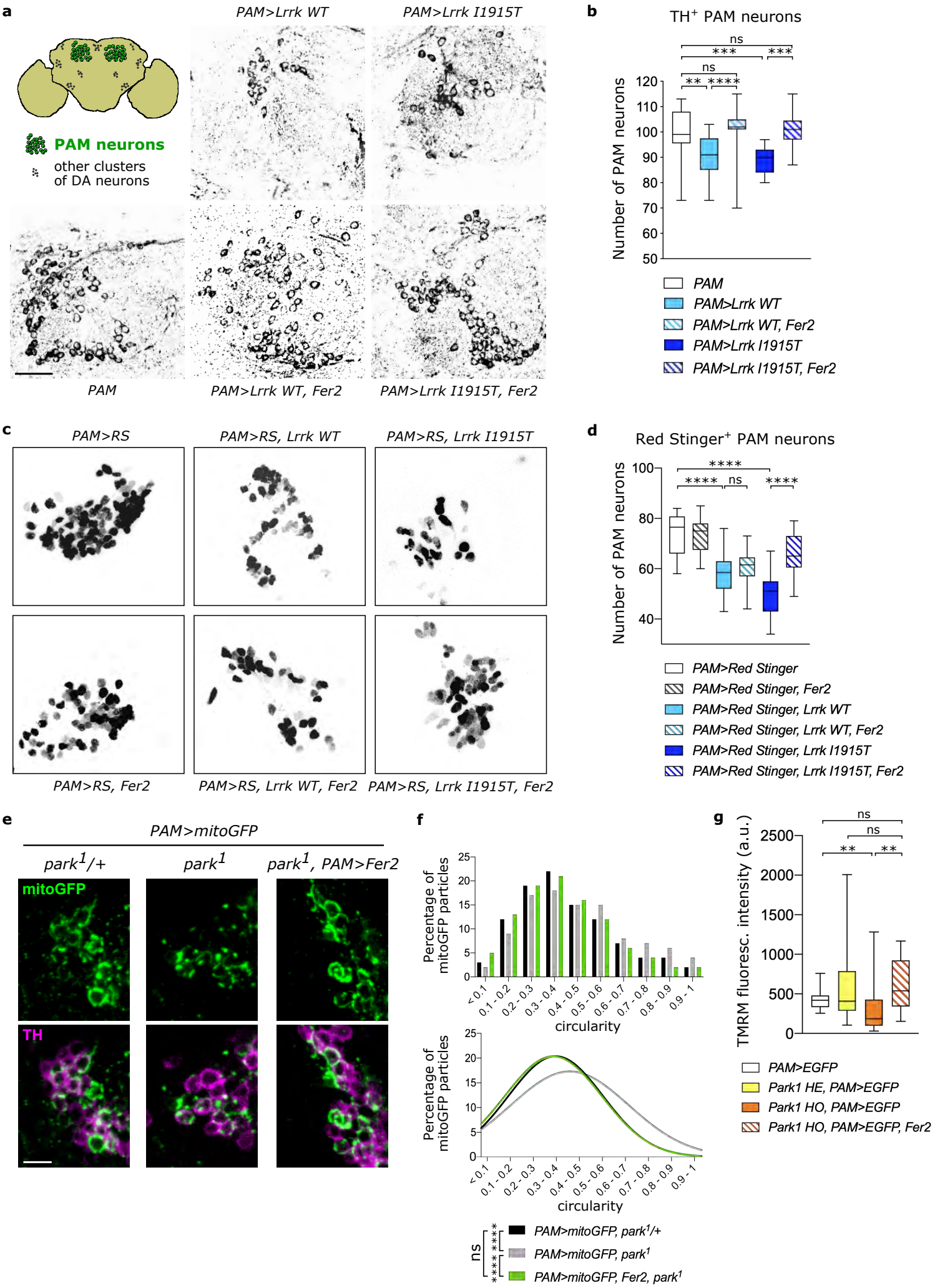
1
a
PAM>Lrrk WT
PAM>Lrrk I1915T
PAM neurons
other clusters of DA neurons
PAM
PAM>Lrrk WT, Fer2
PAM>Lrrk I1915T, Fer2
b
TH+ PAM neurons
Number of PAM neurons
PAM
PAM>Lrrk WT
PAM>Lrrk WT, Fer2
PAM>Lrrk I1915T
PAM>Lrrk I1915T, Fer2
c
PAM>RS
PAM>RS, Lrrk WT
PAM>RS, Lrrk I1915T
PAM>RS, Fer2
PAM>RS, Lrrk WT, Fer2
PAM>RS, Lrrk I1915T, Fer2
d
Red Stinger+ PAM neurons
Number of PAM neurons
PAM>Red Stinger
PAM>Red Stinger, Fer2
PAM>Red Stinger, Lrrk WT
PAM>Red Stinger, Lrrk WT, Fer2
PAM>Red Stinger, Lrrk I1915T
PAM>Red Stinger, Lrrk I1915T, Fer2
e
PAM>mitoGFP
park1/+
park1
park1, PAM>Fer2
mitoGFP
TH
f
Percentage of mitoGFP particles
circularity
PAM>mitoGFP, park1/+
PAM>mitoGFP, park1
PAM>mitoGFP, Fer2, park1
g
TMRM fluoresc. intensity (a.u.)
PAM>EGFP
Park1 HE, PAM>EGFP
Park1 HO, PAM>EGFP
Park1 HO, PAM>EGFP, Fer2

2

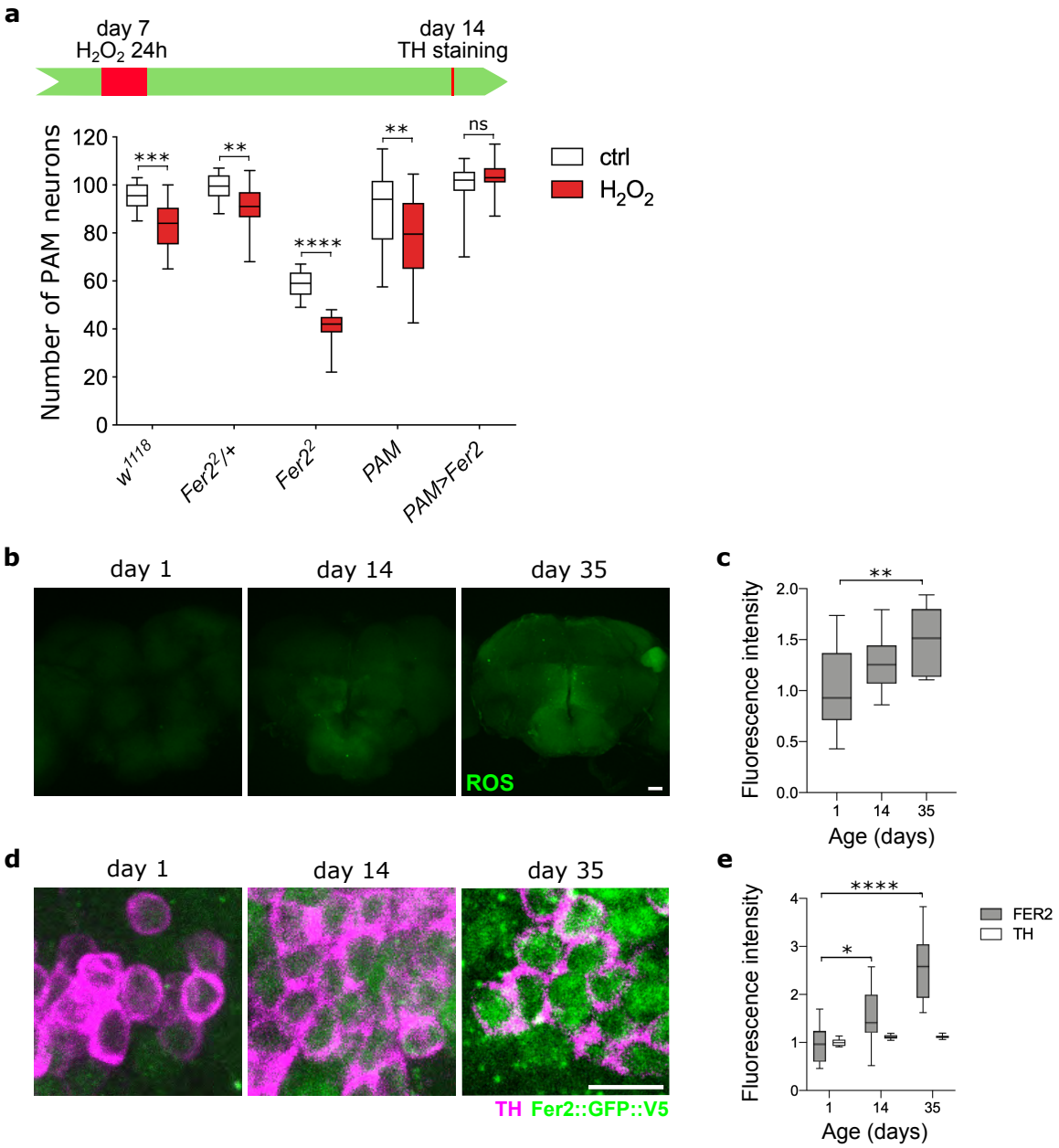
a
day 7
H_2O_2 24h
day 14
TH staining
Number of PAM neurons
120
100
80
60
40
20
0
***
**
****
**
ns
ctrl
H_2O_2
w^{1118}
$Fer2^2/+$
$Fer2^2$
PAM
PAM>Fer2
b
day 1
day 14
day 35
ROS
c
Fluorescence intensity
2.0
1.5
1.0
0.5
0.0
**
1
14
35
Age (days)
d
day 1
day 14
day 35
TH Fer2::GFP::V5
e
Fluorescence intensity
4
3
2
1
0
****
*
FER2
TH
1
14
35
Age (days)

3

a **ChIP-seq**

Fer2::GFP::V5, Fer2[1]

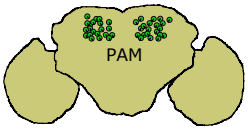

w[1118] (neg ctrl)

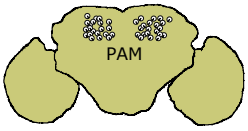

267 peaks
279 associated genes

b

p-value : e^{-42}

c **Head RNA-seq**

hs>Fer2
hs>Fer2 + heat-shock
} DEG after heat-shock induced *Fer2* OE

hs-Gal4
hs-Gal4 + heat-shock
} DEG after heat-shock (independent of *Fer2*)

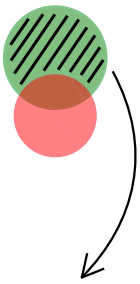

DEG after *Fer2* OE

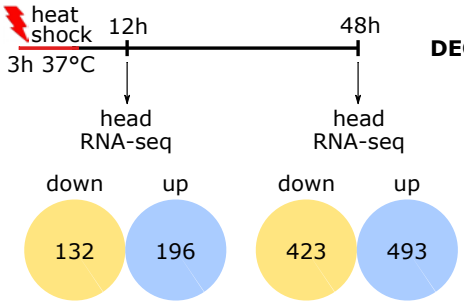

d

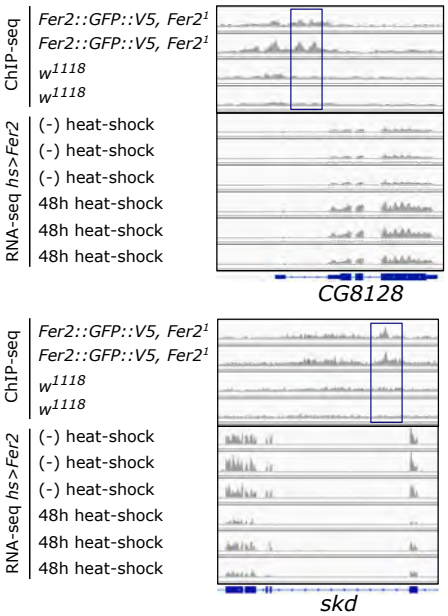

4

a

PAM RNA-seq

PAM>RedStinger ctrl

PAM>RedStinger, Fer2 OE

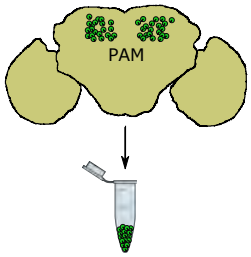

Brain dissociation and isolation of PAM neurons

PAM neuron transcriptome

7134 genes expressed in PAM
132 DEG, p-value<0.01

b

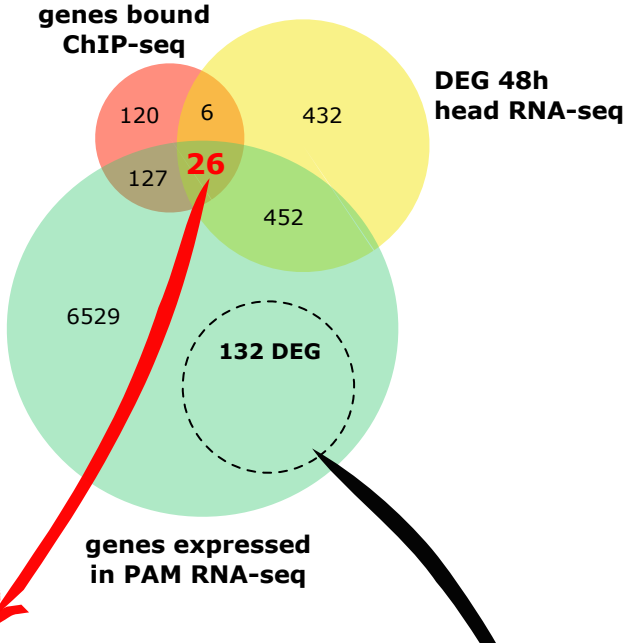

Fer2 direct targets

c

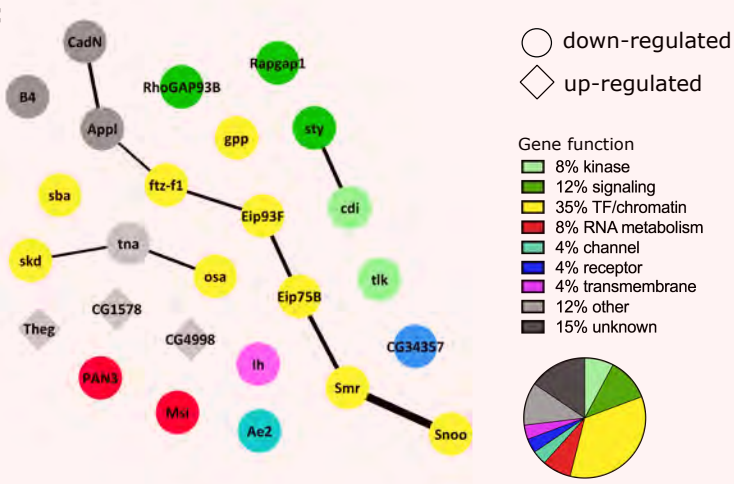

d

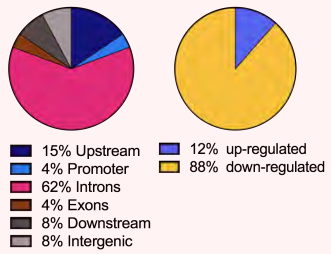

e

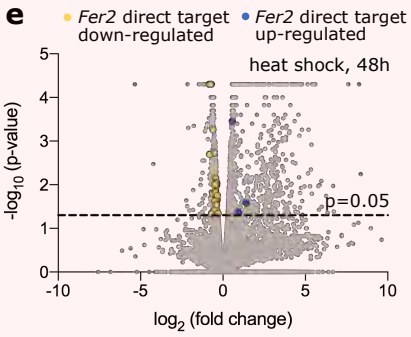

f

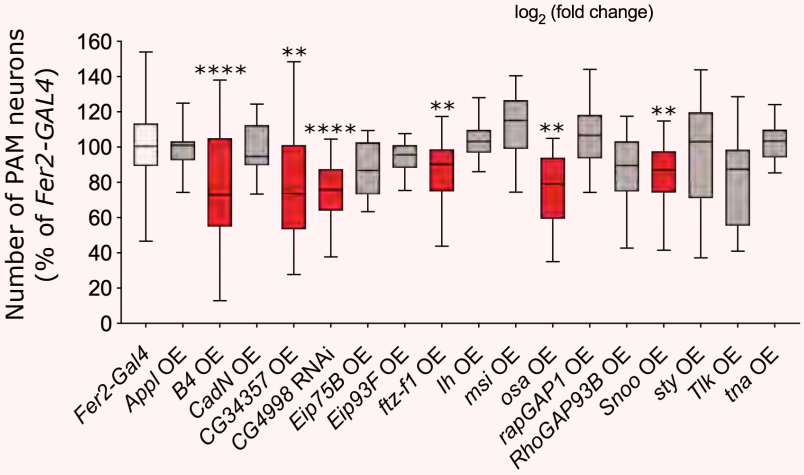

Fer2 secondary targets

g

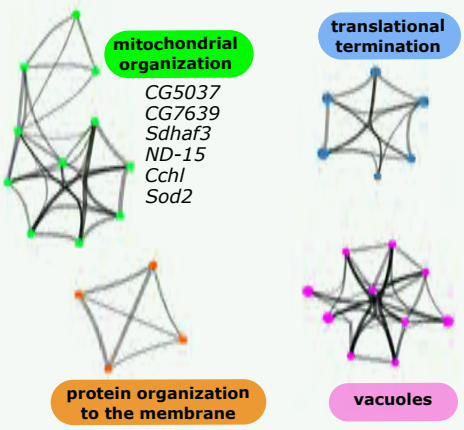

h

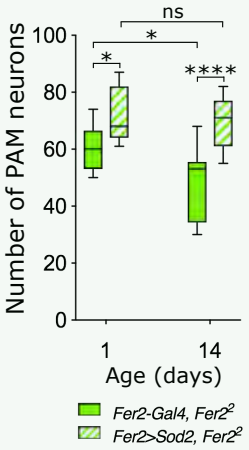

5

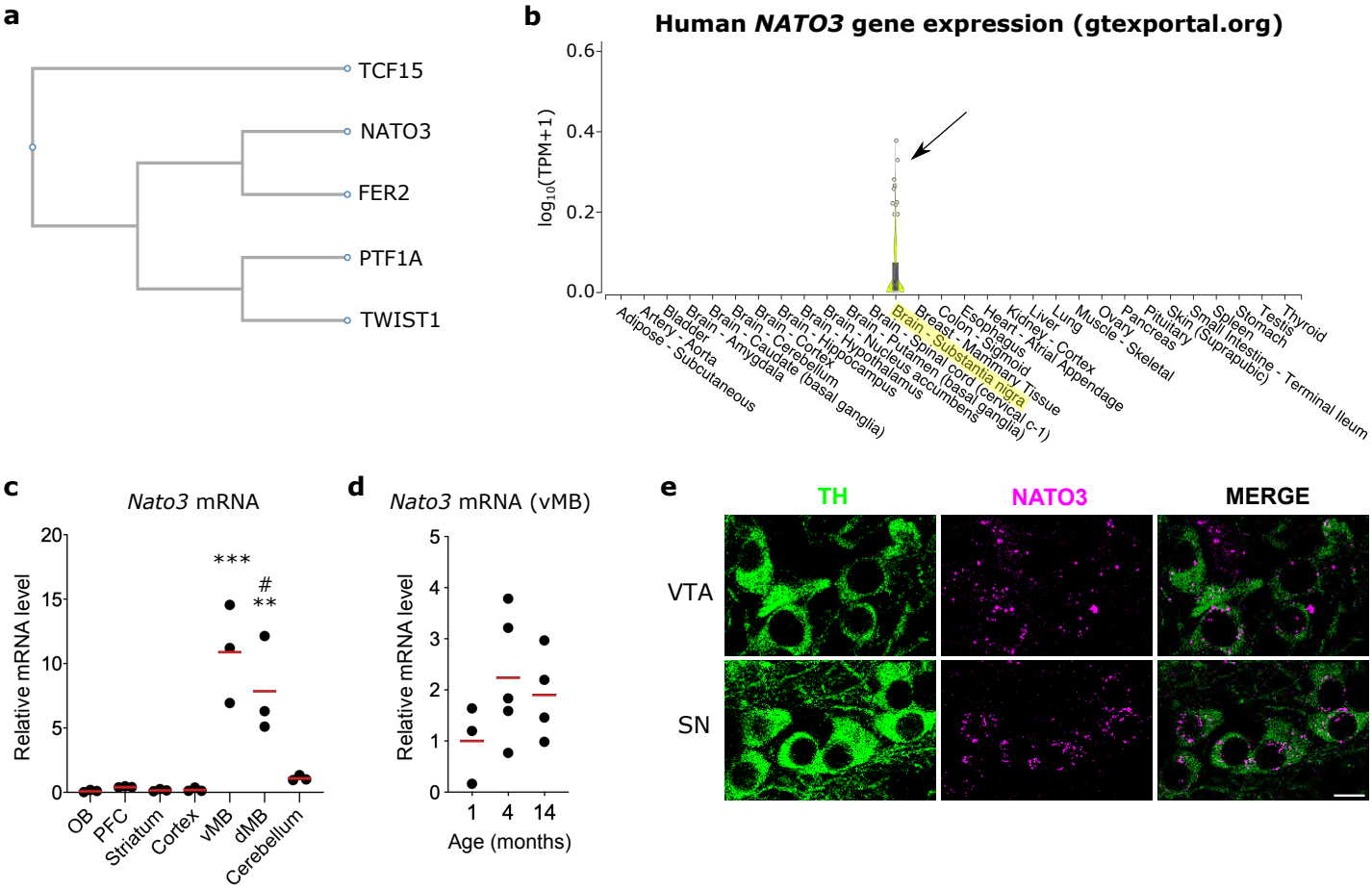
a
TCF15
NATO3
FER2
PTF1A
TWIST1
b
Human NATO3 gene expression (gtexportal.org)
log10(TPM+1)
0.6
0.4
0.2
0.0
Adipose - Subcutaneous
Artery - Aorta
Bladder
Brain - Amygdala
Brain - Caudate (basal ganglia)
Brain - Cerebellum
Brain - Cortex
Brain - Hippocampus
Brain - Hypothalamus
Brain - Nucleus accumbens (basal ganglia)
Brain - Putamen (basal ganglia)
Brain - Spinal cord (cervical c-1)
Brain - Substantia nigra
Breast - Mammary Tissue
Colon - Sigmoid
Esophagus
Heart - Atrial Appendage
Kidney - Cortex
Liver
Lung
Muscle - Skeletal
Ovary
Pancreas
Pituitary
Skin (Suprapubic)
Small Intestine - Terminal Ileum
Spleen
Stomach
Testis
Thyroid
c
Nato3 mRNA
Relative mRNA level
20
15
10
5
0
***
#
**
OB
PFC
Striatum
Cortex
vMB
dMB
Cerebellum
d
Nato3 mRNA (vMB)
Relative mRNA level
5
4
3
2
1
0
1
4
14
Age (months)
e
TH
NATO3
MERGE
VTA
SN

6

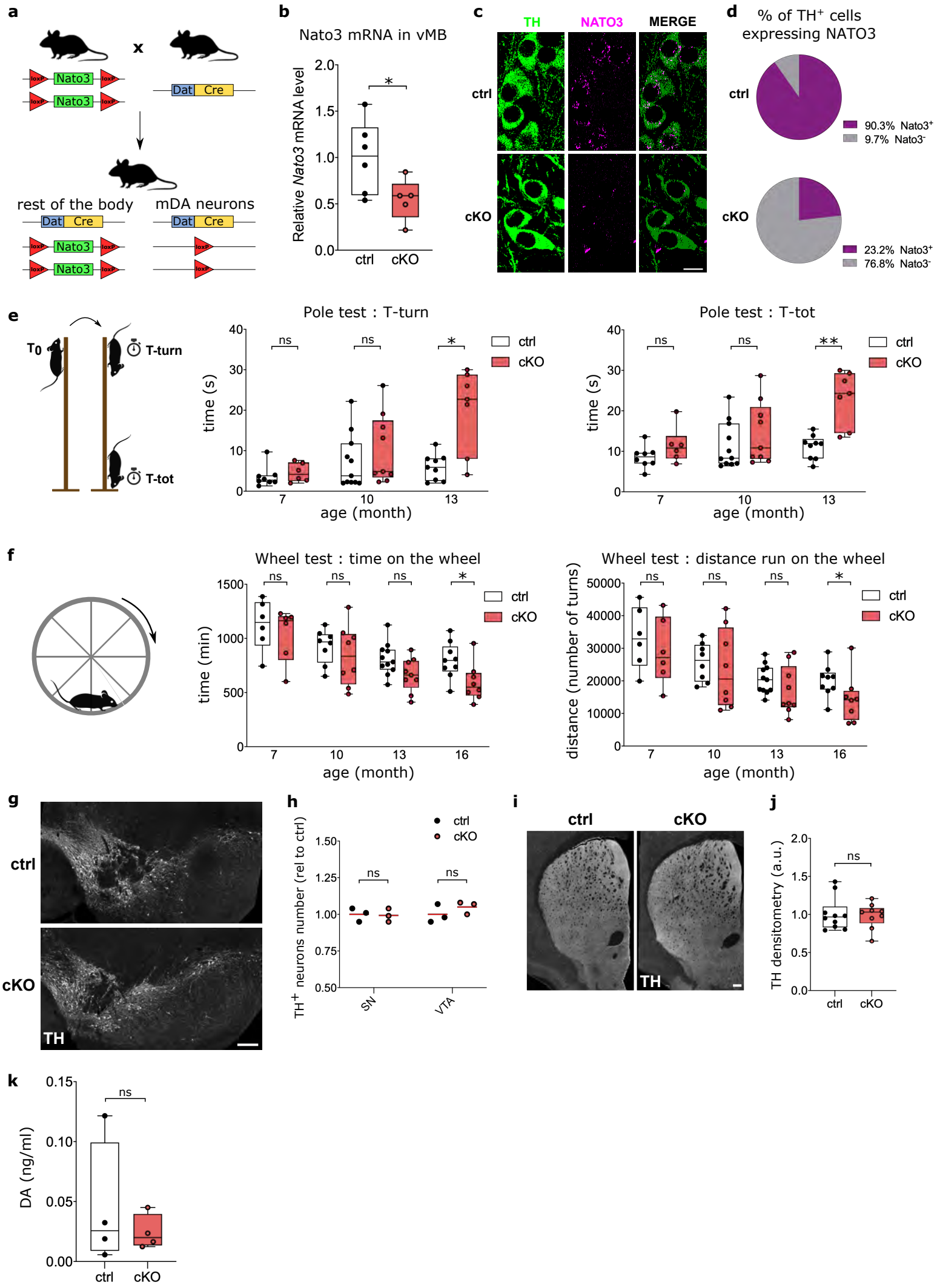
a
x
Nato3
Nato3
Dat
Cre
rest of the body
mDA neurons
b
Nato3 mRNA in vMB
Relative Nato3 mRNA level
ctrl
cKO
c
TH
NATO3
MERGE
ctrl
cKO
d
% of TH+ cells expressing NATO3
ctrl
90.3% Nato3+
9.7% Nato3-
cKO
23.2% Nato3+
76.8% Nato3-
e
T0
T-turn
T-tot
Pole test : T-turn
Pole test : T-tot
time (s)
age (month)
ctrl
cKO
f
Wheel test : time on the wheel
Wheel test : distance run on the wheel
time (min)
distance (number of turns)
age (month)
g
ctrl
cKO
TH
h
TH+ neurons number (rel to ctrl)
SN
VTA
i
ctrl
cKO
TH
j
TH densitometry (a.u.)
k
DA (ng/ml)

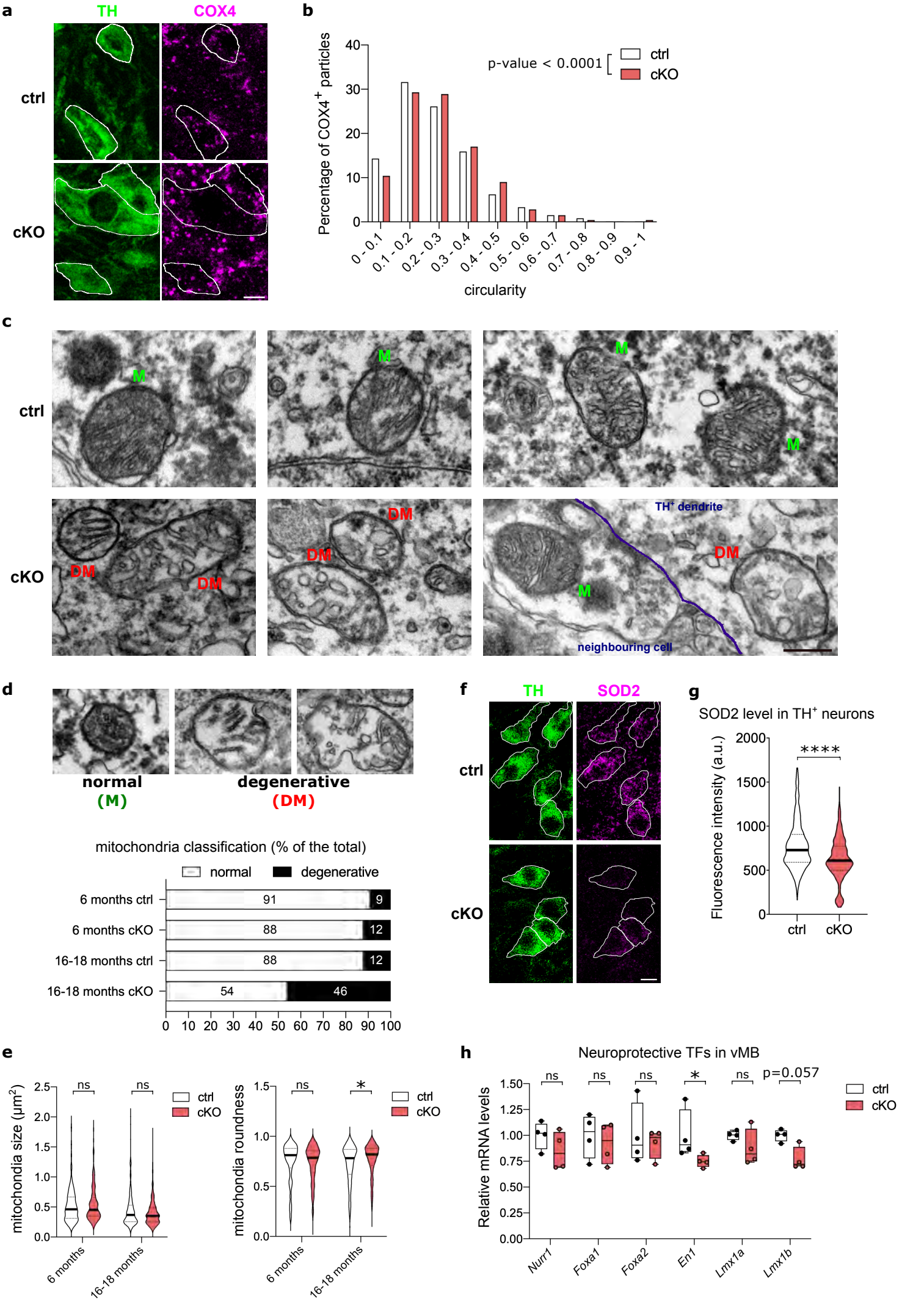
7
a
TH
COX4
ctrl
cKO
b
Percentage of COX4+ particles
p-value < 0.0001
ctrl
cKO
0 - 0.1
0.1 - 0.2
0.2 - 0.3
0.3 - 0.4
0.4 - 0.5
0.5 - 0.6
0.6 - 0.7
0.7 - 0.8
0.8 - 0.9
0.9 - 1
circularity
c
ctrl
cKO
M
DM
TH+ dendrite
neighbouring cell
d
normal
(M)
degenerative
(DM)
mitochondria classification (% of the total)
normal
degenerative
6 months ctrl
6 months cKO
16-18 months ctrl
16-18 months cKO
91
9
88
12
88
12
54
46
f
TH
SOD2
ctrl
cKO
g
SOD2 level in TH+ neurons
Fluorescence intensity (a.u.)
****
ctrl
cKO
e
mitochondia size (μm2)
mitochondia roundness
ns
*
6 months
16-18 months
h
Neuroprotective TFs in vMB
Relative mRNA levels
p=0.057
Nurr1
Foxa1
Foxa2
En1
Lmx1a
Lmx1b